iScience

CellPress
OPEN ACCESS

Article

Pan-cancer noncoding genomic analysis identifies functional *CDC20* promoter mutation hotspots

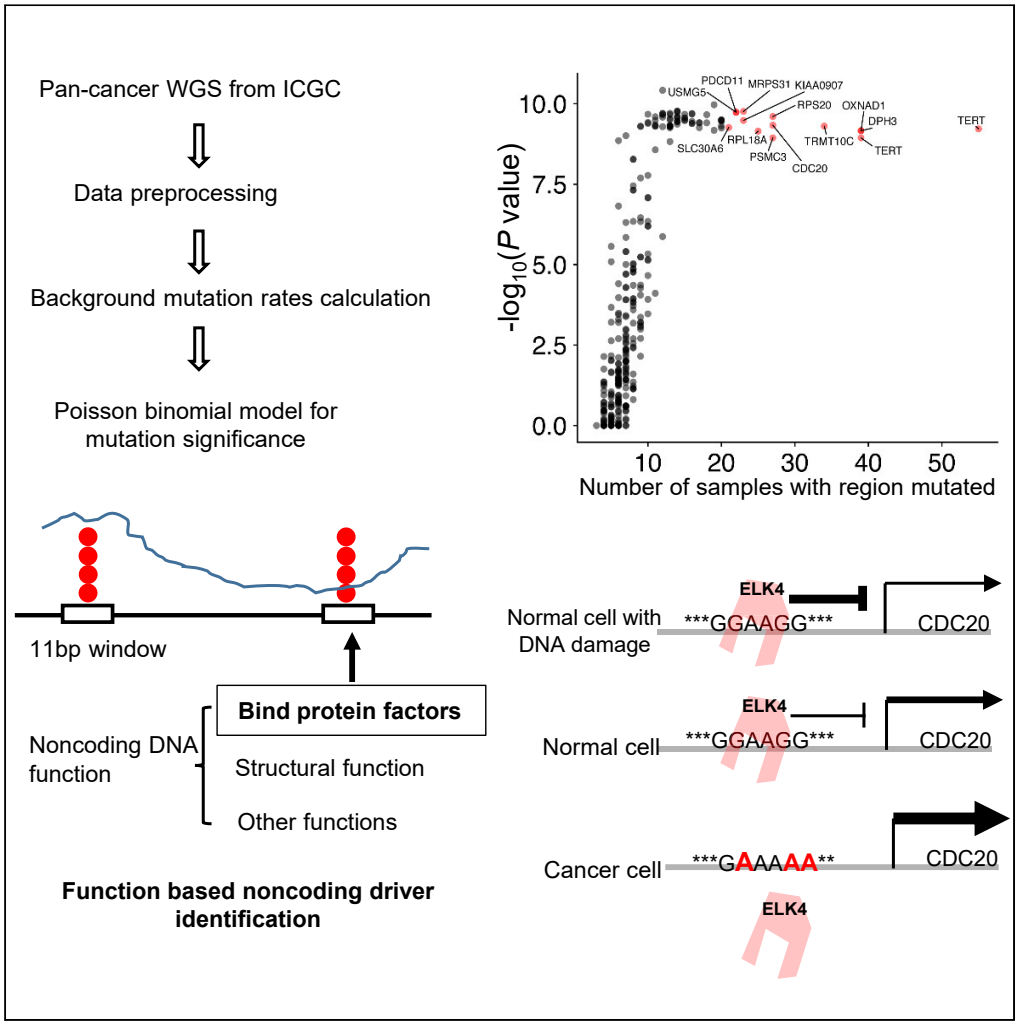

Zaoke He, Tao Wu, Shixiang Wang, ..., Huimin Li, Kai Wu, Xue-Song Liu

liuxs@shanghaitech.edu.cn

Highlights

Pan-cancer noncoding analysis for mutations that influence protein factor binding

Recurrent mutations were identified in the promoter of *CDC20* gene

Promoter hotspot mutations disrupt ELK4 binding, up-regulate *CDC20* transcription

Promoter hotspot mutation site is involved in DNA damage-induced *CDC20* repression

He et al., iScience *24*, 102285
April 23, 2021
https://doi.org/10.1016/j.isci.2021.102285

iScience

CellPress
OPEN ACCESS

Article

Pan-cancer noncoding genomic analysis identifies functional *CDC20* promoter mutation hotspots

Zaoke He,[1,3,4,5] Tao Wu,[1,3,4,5] Shixiang Wang,[1,3,4,5] Jing Zhang,[1,3,4,5] Xiaoqin Sun,[1] Ziyu Tao,[1] Xiangyu Zhao,[1] Huimin Li,[1] Kai Wu,[2] and Xue-Song Liu[1,6,*]

SUMMARY

Noncoding DNA sequences occupy more than 98% of the human genome; however, few cancer noncoding drivers have been identified compared with cancer coding drivers, probably because cancer noncoding drivers have a distinct mutation pattern due to the distinct function of noncoding DNA. Here we performed pan-cancer whole genome mutation analysis to screen for functional noncoding mutations that influence protein factor binding. Recurrent mutations were identified in the promoter of *CDC20* gene. These *CDC20* promoter hotspot mutations disrupt the binding of ELK4 transcription repressor, lead to the up-regulation of *CDC20* transcription. Physiologically ELK4 binds to the unmutated hotspot sites and is involved in DNA damage-induced *CDC20* transcriptional repression. Overall, our study not only identifies a detailed mechanism for *CDC20* gene deregulation in human cancers but also finds functional noncoding genetic alterations, with implications for the further development of function-based noncoding driver discovery pipelines.

INTRODUCTION

Cancer develops primarily because of somatic alterations in the genomic DNA. Somatic mutations in noncoding sequences are poorly explored in cancer, a rare exception being the recent identification of *TERT* promoter mutations (Bell et al., 2015; Horn et al., 2013; Huang et al., 2013). Recently, there have been several research efforts in identifying significantly mutated noncoding sites (Fredriksson et al., 2014; Lochovsky et al., 2015; Melton et al., 2015; Rheinbay et al., 2017; Weinhold et al., 2014; Zhang et al., 2018). Weinhold et al. performed whole-genome sequences (WGS) analysis of 863 pan-cancer samples. Besides *TERT* promoter, some other recurrent promoter mutation hotspots were identified, such as *PLEKHS1*, *WDR74,* and *SDHD* (Weinhold et al., 2014). Fredriksson et al. analyzed 505 tumor genomes across 14 cancer types and identified no other frequent oncogenic promoter mutations beyond *TERT*. It was thus speculated that *TERT* promoter mutation is a rare exception in searching for cancer-driving noncoding genetic alterations (Fredriksson et al., 2014). A recent pan-cancer analysis of whole genomes (PCAWG) study with 2,658 WGS samples also suggested that noncoding drivers are rare compared with protein-coding drivers (Rheinbay et al., 2020).

It has been predicted by the Encyclopedia of DNA Elements (ENCODE) project that roughly 80% of the human genome has biological function (Consortium, 2012). Somatic mutations in noncoding regions are frequent. Disease-associated genomic variations are also frequently located in noncoding regions (Maurano et al., 2012). It is reasonable to expect that cancer should have a substantial number of noncoding driver genetic alterations. However, currently only a few cancer-driving noncoding genetic alterations have been identified, probably because of the following reasons. First, the mutation patterns of noncoding drivers are different from the mutation patterns of coding drivers. Noncoding DNA could have distinct functions: some may code noncoding RNA, some may have structural function, and some may function by binding protein factors. And this is different from coding regions, which function through coding proteins. Consequently, cancer noncoding drivers could have distinct mutation patterns compared with coding drivers, thus requiring distinct methods to identify these noncoding drivers. Second, an insufficient number of patients have been sequenced to identify significantly mutated noncoding elements, especially for those noncoding drivers that occurred at low frequency. Third, there is low sequencing coverage in

[1]School of Life Science and Technology, ShanghaiTech University, Shanghai 201203, China

[2]Department of Thoracic Surgery, The First Affiliated Hospital of Zhengzhou University, Zhengzhou 450052, China

[3]Shanghai Institute of Biochemistry and Cell Biology, Chinese Academy of Sciences, Shanghai, China

[4]University of Chinese Academy of Sciences, Beijing, China

[5]These authors contributed equally

[6]Lead contact

*Correspondence: liuxs@shanghaitech.edu.cn

https://doi.org/10.1016/j.isci.2021.102285

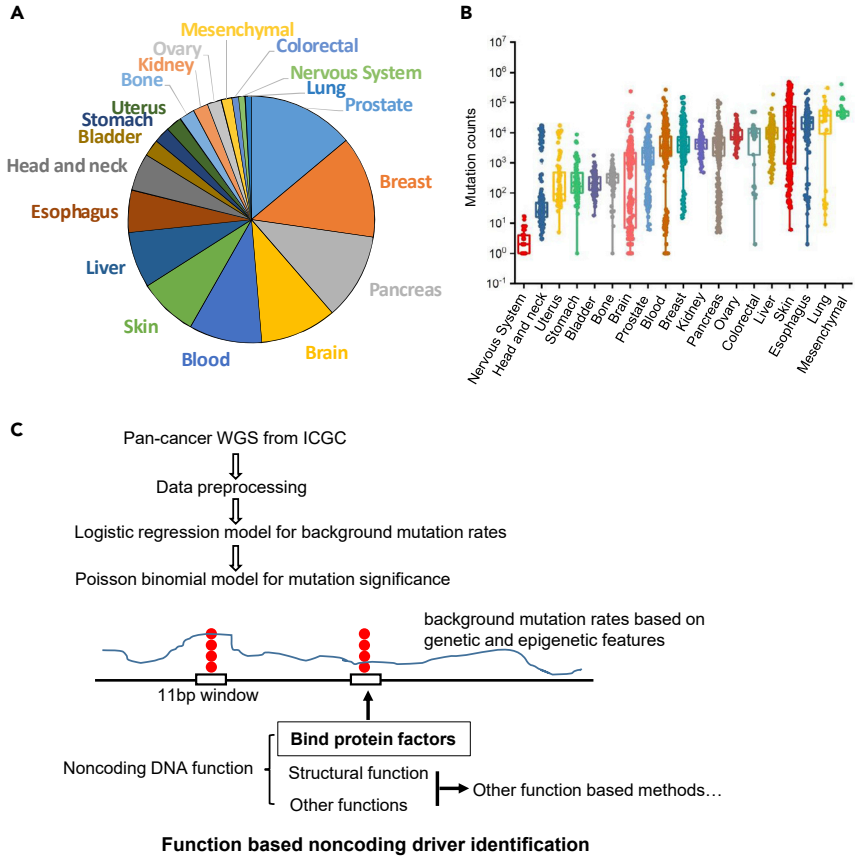

Figure 1. Summary of pan-cancer noncoding analysis data and workflow

(A) Proportion of tumor samples by disease types.

(B) Mutation count distribution of individual samples in 19 cancer types.

(C) Workflow of the method to detect recurrently mutated noncoding regions that affect protein factor binding.

noncoding regions. Owing to sequencing cost, exome sequencing is preferred over WGS in many cancer genomics studies, and noncoding DNA are not covered in these cancer genomic studies. Furthermore, noncoding sequences, especially those that are GC rich or contain repetitive sequences have especially low sequence coverage in second-generation WGS (Rheinbay et al., 2017).

Here we have used so far the largest number of WGS samples to systematically screen for potentially cancer-driving noncoding DNA mutations. Our analysis emphasizes the protein binding function of noncoding sequences. We recapitulated well-known noncoding drivers, such as *TERT* promoter mutations. In addition, we identified novel promoter mutation hotspots in *CDC20*, which is a known cancer-related gene. Further experimental studies supported an oncogenic function of these *CDC20* promoter mutations.

RESULTS

Noncoding mutation analysis of human cancer genome

To obtain the most mutations in genome noncoding regions, we selected patients with tumor with WGS data, filtered out donors with hyper-mutations, and chose single-nucleotide alteration (point mutation) as the focus of this study. Mutations that were potentially false-positive from mapping errors or represented common single-nucleotide polymorphisms were removed from further analysis. After filtering, WGS data of 4,859 donors from 19 cancer types have been included in this study (Figures 1A and S1). The average mutation count for the overall sample is 9,819, and in total 47,708,263 mutations have been included in this study. The distribution of mutation counts in each sample is shown, and most samples have mutation counts less than 20,000 (Figure 1B). There are big differences in mutation burdens between cancer types or between samples with the same cancer type (Figure 1B).

To identify the factors that influence background mutation rates, we performed correlation analysis between genetic and epigenetic features with background mutation rates. It has been reported that mutation rates in cancer genomes are highly correlated with chromatin organization status, and the arrangement of the genome into heterochromatin- and euchromatin-like domains is a dominant influence on regional mutation-rate variation in human somatic cells (Schuster-Bockler and Lehner, 2012). Here we analyzed the correlations between genetic or epigenetic features and mutation rates in coding and noncoding regions (Figure S2A). The following genetic features have been included in this analysis: genome mappability, replication timing, transcription factor binding sites (TFBS), GC content, CpG island, DNA polymerase II, DNA conservation, and recombination rate. The following epigenetic features were also included: DNase I hypersensitive site and histone modifications (H3K4me1, H3K4me3, H3K27me3, H3K36me3, H3K9me3, H3K27ac, and H3K9ac). We then calculated the correlation coefficients for all genetic or epigenetic features with background mutation rates and found that at the megabase scale, cancer noncoding mutation rates show strong correlation with several features of chromatin structure (Figure S2B). Heterochromatin markers H3K27me3 and H3K9me3 are associated with increased noncoding mutation rates (Figure S2B). TFBS show elevated mutation rates (Mao et al., 2018) (Figure S2D). Furthermore, these correlations in noncoding regions are similar to the correlations in coding regions (Figures S2B and S2C), suggesting that the background mutation rates in both coding and noncoding regions are similarly influenced by these genetic or epigenetic features.

Pan-cancer genomic analysis to identify noncoding mutation hotspots

To identify positive selection in cancer genomes, it is essential to build an accurate background mutation rate model that corrects for covariates (features) that impact regional mutation rate variation, such as local sequence context and chromatin features (Schuster-Bockler and Lehner, 2012). Our algorithm employed logistic regression to determine sample-specific and covariate-corrected background mutation probabilities followed by a Poisson binomial model to account for patient-specific probabilities (Figures 1C and S3). Logistic regression was performed to calculate the expected probability (or background probability) for each genome site. We considered a range of genetic and epigenetic features that correlated with somatic noncoding mutation rates, including genetic features (sequence context, replication timing, TFBS, conservation, GC content, CpG density, promoter) and epigenetic features (DNase I hypersensitive site and histone modifications H3K4me1, H3K4me3, H3K27me3, H3K36me3, H3K9me3, H3K27ac, and H3K9ac).

Non-protein-coding DNA elements could have the following potential functions: code for non-protein-coding RNA, act as *cis*-regulatory elements, or serve for some unknown structural function. The *cis*-regulatory elements include proximal regulatory elements (promoters, etc.) and distal elements (enhancers, silencers, insulators, etc.). Most of these *cis*-regulatory noncoding DNA elements function through binding protein factors. Here we developed an analysis framework that emphasized the protein binding function of noncoding DNA sequences (Figure 1C). To identify noncoding mutations that could have potentially functional consequence in protein binding, we focused on clustered mutation hotspots. As most protein factors bind DNA 6–10 bp long, the clustered regions were defined as a 10-bp DNA surrounding the recurrently mutated sites. The probability that mutation happened in this 11-bp window was calculated with a Poisson binomial distribution model. Noncoding mutations in promoter regions (within 5 kb of gene transcription start sites) were further selected in downstream analysis and experimental validation.

We ranked the selected 11-bp noncoding regions based on calculated mutation probability and mutation frequency (Figure 2A), and *TERT* promoter mutations are top ranked (Figures2A and S4). Some of the previously reported significantly mutated promoters were identified, such as *DPH3* promoter mutations (Denisova et al., 2015) (Figure 2B). In addition, some novel noncoding mutation hotspots were also identified, including promoter mutations of *RPL18A* (Figure 2B). Patients with melanoma with hotspot mutations in *RPL18A* promoter have significantly poorer prognoses compared with patients without those hotspot mutations (Figure S5). The function of most of these identified noncoding mutations is unknown. Interestingly, we identified novel recurrent clustered mutations in the promoter region of *CDC20* gene (Figure 2B and Table S1). Similar analyses were performed with the selection of different window sizes from 7 to 21 bp, and *CDC20* promoter mutations are top ranked in all these analyses (Figure S6). To identify mutational clusters in noncoding regions in liver cancer, Fujimoto et al. selected a 500-bp window to calculate the statistical significance (Fujimoto et al., 2016). The significantly mutated regions identified with these larger windows may not directly influence the binding of protein factors. Recurrent indels in the promoter regions are shown (Figure S7), and clustered mutations in 3′-UTR, 5′-UTR, and intron regions are also shown (Figure S8).

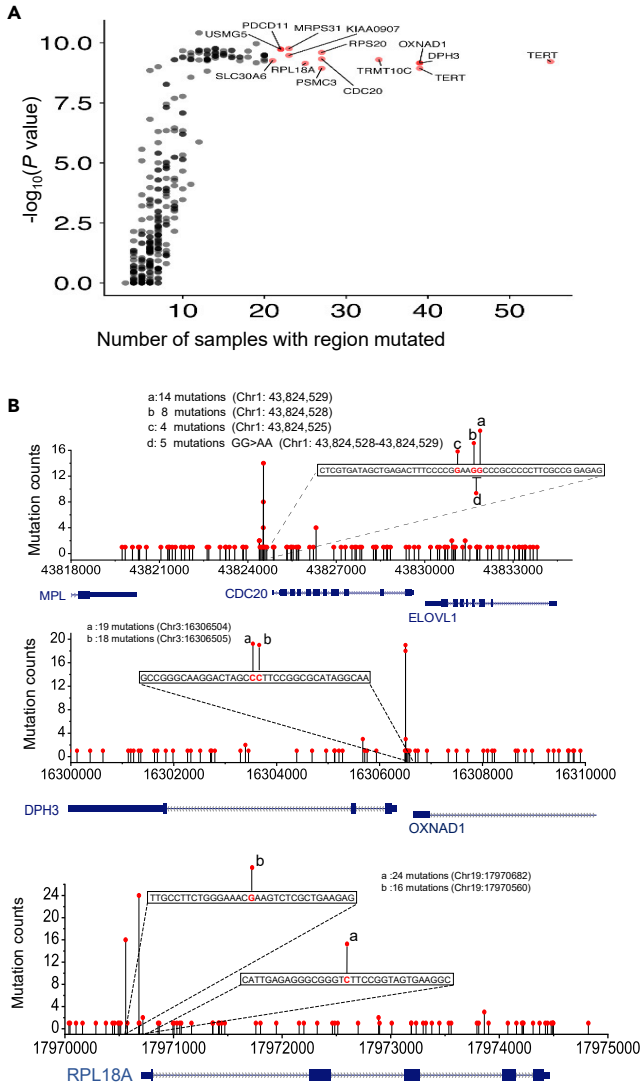

Figure 2. Noncoding mutation hotspots analysis

(A) Shown is the probability ($-\log_{10}$) of noncoding mutations in the 11-bp window (y axis) plotted against the number of times the noncoding region is found mutated (x axis). Bonferroni-adjusted p values are shown.

(B) Typical noncoding mutation hotspots in regulatory regions of *CDC20*, *DPH3*/*OXNAD1*, and *RPL18A* genes are shown.

Genetic alterations of *CDC20* in human cancers

CDC20 was discovered in the early 1970s when Hartwell et al. made yeast mutants that failed to complete cell cycle progression (Hartwell et al., 1970). The *CDC20* mutant could not enter anaphase (Hartwell et al., 1973). In 1995, the biochemical function of *CDC20* became clear after the discovery of the APC/C (King et al., 1995; Sudakin et al., 1995). The APC/C-CDC20 protein complex plays a key role in cell cycle spindle checkpoint and metaphase-to-anaphase transition mainly through two protein targets. First, it targets securin for destruction, enabling the eventual destruction of cohesin and thus sister chromatid separation. It also targets cyclins for destruction, which inactivates cyclin-dependent kinases (Cdks) and allows the cell to exit from mitosis (Pesin and Orr-Weaver, 2008).

Previous studies reported that *CDC20* is overexpressed in various human cancers (Chang et al., 2012; Gayyed et al., 2016; Kim et al., 2014; Wang et al., 2013). We systematically compared the mRNA expression of *CDC20* between cancer and normal tissues in various cancers based on TCGA datasets. In nearly all types of cancers analyzed, elevation of *CDC20* mRNA expression is observed (Figure 3A). These data validated

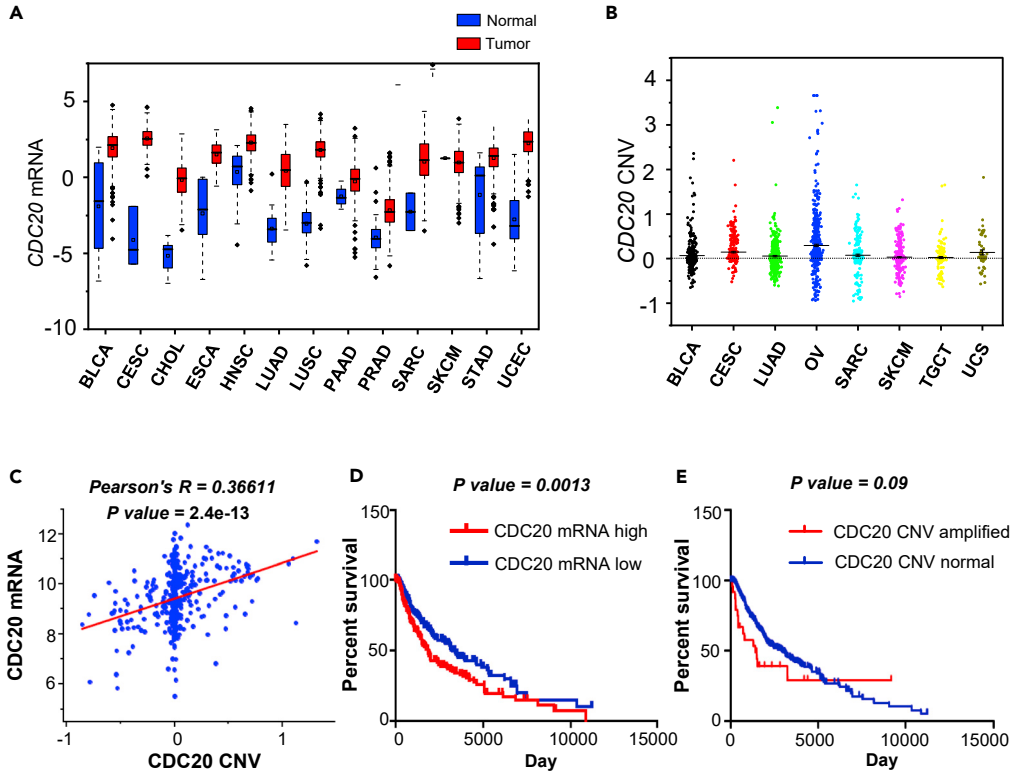

Figure 3. mRNA and CNV analysis of *CDC20* in various human cancers

(A) *CDC20* mRNA expression levels were compared in multiple types of human cancers and corresponding normal control tissues based on The Cancer Genome Atlas (TCGA) database. The boxplot is bounded by the first and third quartiles with a horizontal line at the median.

(B) *CDC20* CNV levels in various cancers are shown based on TCGA datasets. The unit is Gistic2 copy number.

(C) The correlation between *CDC20* CNV and mRNA in TCGA melanoma samples (n = 367). Pearson correlation P and *R* values are shown.

(D and E) Kaplan-Meier overall survival curves of patients with melanoma are shown. Patients are separated into two groups based on *CDC20* mRNA (D) or CNV (E) values. n = 231 for both *CDC20* mRNA high and low groups. n = 24 for *CDC20* CNV amplified group and n = 333 for CDC20 CNV normal group. Log rank (Mantel-Cox) test p values are shown. BLCA: bladder cancer; CESC: cervical cancer; CHOL: bile duct cancer; ESCA: esophageal cancer; HNSC: head and neck cancer; LUAD: lung adenocarcinoma; LUSC: lung squamous cell carcinoma; PAAD: pancreatic cancer; PRAD: prostate cancer; SARC: sarcoma; SKCM: melanoma; STAD: stomach cancer; UCEC: endometrioid cancer. OV: ovarian cancer; TGCT: testicular germ cell tumors; UCS: uterine carcinosarcoma.

previous observations. Recurrent genetic alterations are typical features of cancer-driving genes. We further analyzed genetic alterations in *CDC20* genes based on public cancer genome databases. No recurrent somatic mutations in *CDC20* coding sequence were identified. However, the copy number variation (CNV) of *CDC20* shows amplification in various cancers including ovarian cancer, bladder cancer, cervical cancer, etc (Figure 3B). *CDC20* CNV shows significant positive correlation with *CDC20* mRNA (Figure 3C). Genetic amplification of *CDC20* suggests an oncogenic driving function of *CDC20* in cancer progression.

It has been reported that overexpression of *CDC20* promoted cancer progression, whereas its knockdown suppressed cancer (Majumder et al., 2014; Mukherjee et al., 2013). *CDC20* was suggested as a legitimate target of drug development for the treatment of human malignancies (Wang et al., 2013). We studied the prognosis of *CDC20* mRNA expression in melanoma. As previously reported, *CDC20* mRNA overexpression leads to significantly poorer melanoma prognosis (Figure 3D). *CDC20* CNV amplification also tends to result in poorer melanoma prognosis (Figure 3E). Taken together, these data support an oncogenic driving function of *CDC20* in human cancer. The CNV amplification and mRNA up-regulation of *CDC20* in cancer versus normal is one rationale for us to further investigate the function of these *CDC20* promoter noncoding hotspot mutations.

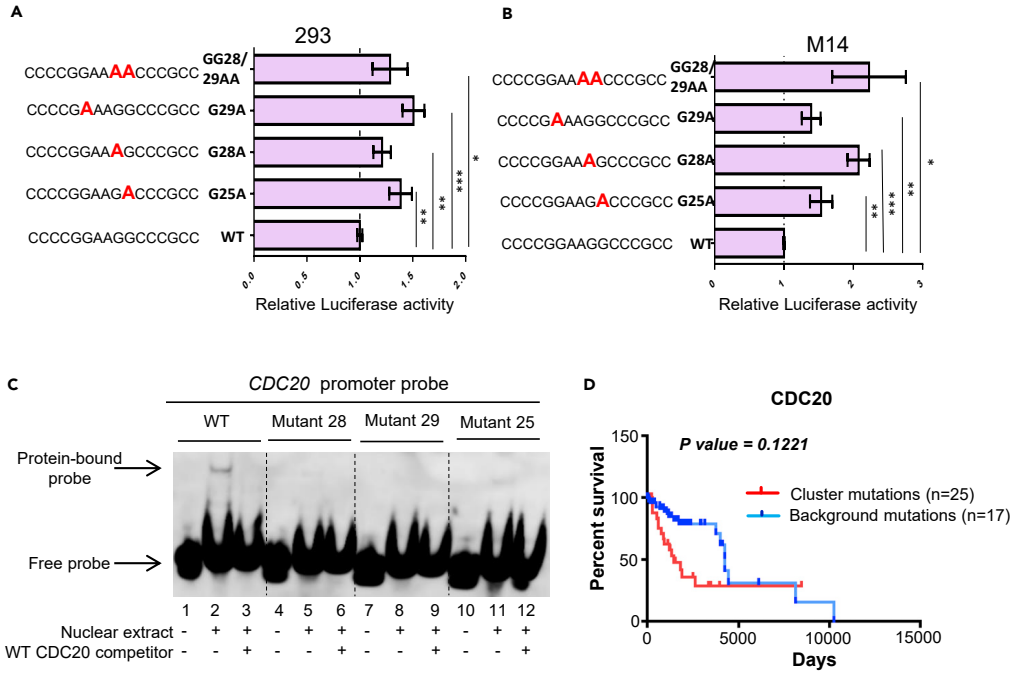

Figure 4. Functional consequence of *CDC20* promoter hotspot mutations

(A and B) Luciferase reporter assay was performed in 293 (A) and M14 cells (B) with wild-type (WT) or mutant *CDC20* promoter driving luciferase vectors. Error bars represent mean ± SD from three experiments. *p < 0.05, **p < 0.01, ***p < 0.001. Unpaired Student's t test p values between each mutation and WT control are shown.

(C) EMSA assays were performed with wild-type or mutant *CDC20* promoter probes. *CDC20* promoter mutation strongly abolish protein factor binding to DNA probes.

(D) Kaplan-Meier overall survival curves of patients with melanoma with indicated *CDC20* promoter mutations or control mutations. n = 25 for patients with clustered *CDC20* promoter mutations (including G25A, G28A, G29A, and GG28/29AA), n = 17 for patients with other mutations in the background region. Log rank (Mantel-Cox) test p value is shown.

Recurrent promoter mutations stimulate *CDC20* transcription

To test whether the mutations identified in *CDC20* promoter region have functional consequence, we used luciferase reporter assay to evaluate the effect of each mutation on *CDC20* promoter activity. It has been reported that endogenous *CDC20* transcription can be suppressed by DNA damage drugs, such as 5-fluorouracil (5-FU) (Banerjee et al., 2009). To test if the luciferase reporter we generated can mimic the activity of endogenous *CDC20* promoter, we studied the response of our luciferase reporter to 5-FU treatment. Similar to endogenous *CDC20* promoter, the activity of the luciferase reporter was down-regulated after 5-FU treatment (Figure S9). In two cell types (293, M14) tested, recurrent *CDC20* promoter mutations (including: G25A, G28A, G29A, and GG28/29AA) lead to significantly elevated promoter activity (Figures4A and 4B). However, randomly selected mutation around the consensus sites did not influence luciferase activity (Figure S10). In patient samples with mRNA expression data available (6 samples with *CDC20* promoter hotspot mutation, 27 samples without hotspot mutation), *CDC20* mRNA tend to be up-regulated in melanoma samples with the promoter hotspot mutation (Figure S11) and the difference does not reach statistical significance (unpaired Student's t-test, p = 0.25), probably due to the limited sample size. Electrophoretic mobility shift assays (EMSA) were performed to analyze changes in protein binding between wild-type and mutant promoters. Results indicate that all tested recurrent *CDC20* promoter mutations have compromised binding affinity to protein factors (Figure 4C).

The four recurrent mutation hotspots in *CDC20* promoter may constitute a single functional protein binding DNA site. Most of the *CDC20* promoter hotspot mutations are identified in patients with melanoma. The prognosis of patients with melanoma with the mentioned *CDC20* promoter hotspot mutations was poorer compared with that of patients without these mutations (Figures 4D and S12); the differences do not reach statistical significance probably due to limited sample size. This implies a function of these *CDC20* promoter mutation hotspots in cancer progression.

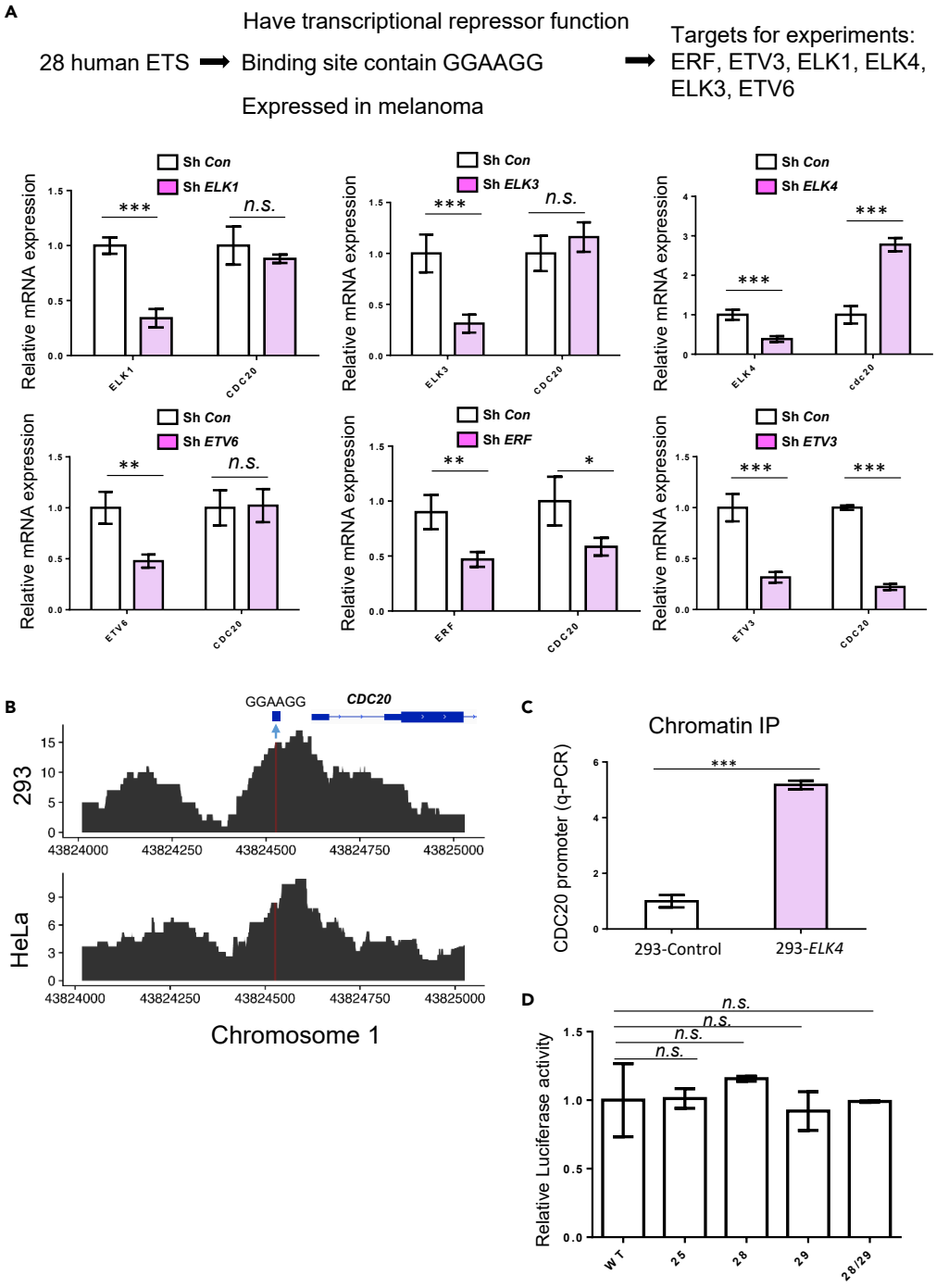

Figure 5. ELK4 binds to the hotspot mutation targeted sequence and represses *CDC20* transcription

(A) Screen for ETS proteins that bind the hotspot mutation targeted sequence "GGAAGG" and repress *CDC20* transcription. shRNA experiments were performed in 293 cells; expression of each ETS and *CDC20* mRNA was quantified by qPCR. *p < 0.05, **p < 0.01, ***p < 0.001, Student's t test compared to sh-control. The results are an average of three independent experiments. Values are mean ± SD.

(B) ENCODE ELK4 ChIP-seq data around the hotspot mutation target sequence "GGAAGG" in 293 and HeLa cells.

(C) ChIP was performed with anti-FLAG antibody in M14 cells stably expressing FLAG-ELK4 or FLAG control. The DNA sequence around the hotspot mutation target sequence was quantified with qPCR. ***p < 0.001,

Figure 5. *Continued*
Student's t test compared with FLAG control. The results are an average of three independent experiments. Values are mean ± SD.
(D) Luciferase reporter assay was performed in *ELK4* knockdown 293 cells with wild-type or mutant *CDC20* promoter driving luciferase vectors. The results are an average of three independent experiments. Values are mean ± SD.

ELK4 binds to the unmutated sequence and represses *CDC20* transcription

The hotspot mutations in *CDC20* promoter are located in the DNA motif GGAAGG, which is predicted to be the binding site for the E26 transformation-specific (ETS) family transcription factors. Mutations in this motif consequently disrupt the binding of ETS transcription factors. To date, 28 ETS transcription factors have been reported in humans (Sizemore et al., 2017). We screened for the potential protein factors that bind to the *CDC20* promoter hotspot mutation-targeted DNA motif based on the following three criteria: (1) the binding sites of the potential transcription factors contain GGAAGG, (2) the potential transcription factors function as transcription repressors, and (3) the potential transcription factors are expressed in melanoma samples. In 28 ETS transcription factors, only six (ERF, ETV3, ELK1, ELK4, ELK3, ETV6) meet the above-mentioned three criteria. Then we experimentally tested the function of these six transcription factors in *CDC20* transcriptional regulation.

We designed short hairpin RNA (shRNA) to knock down the expression of each of the six transcription factors, then checked the expression of *CDC20*, and observed that only knockdown of *ELK4* but not the other five transcription factors resulted in significant up-regulation of *CDC20* transcription (Figure 5A). These data suggest that ELK4 could be the transcription factor that binds to the hotspot mutation targeted motif and suppresses *CDC20* transcription. Based on public ENCODE chromatin immunoprecipitation sequencing (ChIP-seq) datasets, ELK4 binds *CDC20* promoter DNA sequence, and the mutation hotspots are located close to the peak of ELK4 ChIP-seq signals (Figures 5B and S13). The binding between ELK4 and *CDC20* promoter DNA sequence has been experimentally validated with ChIP in M14 cell line (Figure 5C).

In several different cell lines, overexpression of *ELK4* leads to the down-regulation of *CDC20* transcription and knockdown of *ELK4* results in the up-regulation of *CDC20* transcription (Figures S14 and S15). Furthermore, knockdown of *ELK4* can diminish the effects of hotspot mutations on *CDC20* transcription (Figure 5D). These experimental evidences suggest that ELK4 can be the transcription factor that binds the hotspot mutations targeted sequence and suppresses the transcription of *CDC20*.

Hotspot mutation targeted sequence mediates DNA damage-induced *CDC20* transcription repression

CDC20 forms a complex with APC/C, and plays a key role in cell cycle spindle checkpoint and metaphase-to-anaphase transition. One of the key physiological functions of APC/C-CDC20 complex is to check the integrity of genome, and DNA damage signal has been reported to dramatically suppress the transcription of *CDC20* (Banerjee et al., 2009). However, the detailed molecular mechanism for this DNA damage-induced *CDC20* transcriptional repression is not clearly understood.

We investigated the consequence of the hotspot mutations on DNA damage-induced *CDC20* transcriptional repression. Using a luciferase reporter assay, the hotspot mutations significantly compromised the effect of DNA damage drug 5-FU on *CDC20* transcriptional suppression (Figures 6A and 6B). This suggested a function of these hotspot mutation targeted sequences in DNA damage-induced *CDC20* transcriptional suppression. *ELK4* knockdown with shRNA also diminishes the effects of hotspot mutations on DNA damage-regulated *CDC20* transcriptional repression (Figure 6C). These experimental evidences suggested that the physiological function of ELK4 binding to the hotspot mutation targeted sequence could be DNA damage-induced *CDC20* transcriptional repression (Figure 6D).

DISCUSSION

To identify potentially cancer-driving noncoding mutations, we performed pan-cancer WGS analysis with 4,859 samples, the largest number of WGS samples included thus far. We validated known recurrent noncoding mutations. In addition, we identified novel noncoding mutation hotspots, including *CDC20* promoter mutation hotspots, which have been further studied by experiments.

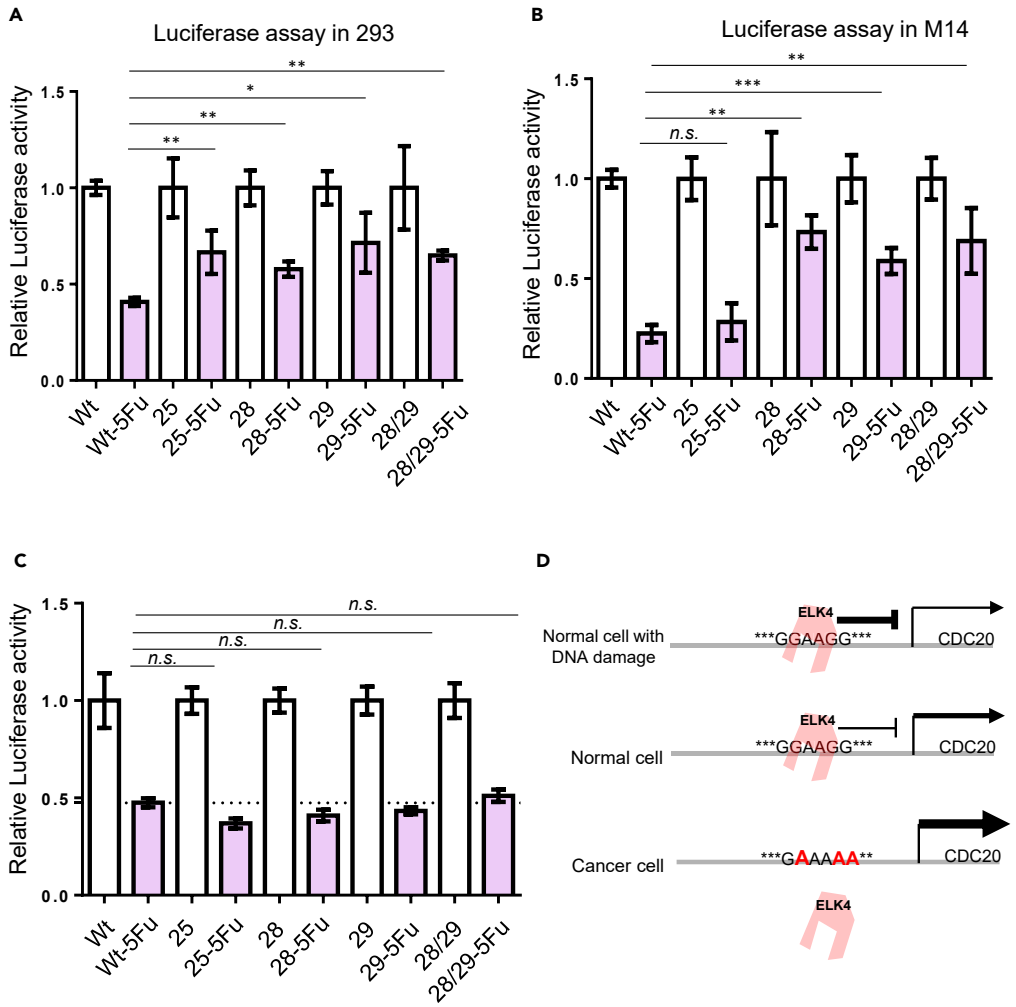

Figure 6. Hotspot mutation targeted sequence mediates DNA damage-induced *CDC20* transcriptional repression

(A and B) Luciferase reporter assay was performed in 293 (A) or M14 (B) cells with wild-type or mutant *CDC20* promoter driving luciferase vectors in the presence or absence of DNA damage drug 5-FU. *p < 0.05, **p < 0.01, ***p < 0.001, Student's t test compared with wild-type. The results are an average of three independent experiments. Values are mean ± SD.

(C) Luciferase reporter assay was performed in *ELK4* shRNA knockdown 293 cells with wild-type or mutant *CDC20* promoter driving luciferase vectors in the presence or absence of 5-FU.

(D) Proposed function for the hotspot mutation targeted sequence in *CDC20* transcriptional regulation.

Several recent pan-cancer noncoding studies suggested that cancer noncoding drivers are rare compared with coding drivers (Fredriksson et al., 2014; Rheinbay et al., 2020). One reason might be that these methods did not consider the distinct mutation pattern of noncoding drivers due to the distinct function of noncoding DNA. Many noncoding DNAs act as *cis*-acting element and function by binding protein factors. Our noncoding analysis framework focused on this protein binding function of noncoding DNA. In addition to binding protein factors, noncoding DNA can have a variety of other functions. Some noncoding sequences could have structural function in nucleus organization. For this type of noncoding mutation, we need to focus on the structural effects of genetic alterations. For example, noncoding DNA with a long linear distance can form functional units through 3D interactions, and this type of noncoding driver cannot be identified through conventional linear-based significance analysis. Overall, cancer-driving noncoding mutations may have a different mutation pattern due to different functions. Distinct methods should be applied for identifying those noncoding DNA alterations with distinct functional impacts. However, current

methods of cancer noncoding driver discovery did not consider these structural and other functional impacts of noncoding DNA alteration, so it is very likely that many functional noncoding cancer drivers still remain to be discovered.

CDC20 is a well-known key player in cell cycle regulation. Its expression is frequently up-regulated in various human cancers (Chang et al., 2012; Gayyed et al., 2016; Kim et al., 2014; Wang et al., 2013). Overexpression of *CDC20* is correlated with clinicopathological parameters of various cancers (Wang et al., 2013). *CDC20* inhibitors are in development for the treatment of human cancers (Jiang et al., 2012; Zeng et al., 2010). Importantly, anti-mitotic agents including taxol and nocodazole, which have long been utilized as anticancer reagents, could function by inhibiting APC/C-CDC20 (Huang et al., 2009).

Most of the hotspot mutations in *CDC20* promoter are identified in melanoma samples. Melanoma genomes are known to have high mutation load compared with other cancer types and a predominant C>T nucleotide transition signature attributable to UV radiation (Alexandrov et al., 2013). ETS binding sites in promoter regions are vulnerable to UV mutagenesis (Fredriksson et al., 2017). It is highly possible that these *CDC20* promoter hotspot mutations and other hotspot mutations in melanoma are generated by UV; however, this does not exclude the possibility that some hotspot mutations in transcription factor binding sites can still be functional in cancer evolution, and these need to be tested by experiments. Here we experimentally demonstrated that the *CDC20* promoter hotspot mutations disrupt the binding of transcriptional repressor ELK4, and consequently up-regulate the transcription of *CDC20*. *CDC20* is known to have cancer-driving function through the regulation of cell cycle progression, and consistently *CDC20* expression is ubiquitously up-regulated in various cancer types (Chang et al., 2012; Gayyed et al., 2016; Kim et al., 2014; Wang et al., 2013) (Figure 3A). Thus, the promoter hotspot mutations reported here can promote cancer progression by up-regulating the transcription of *CDC20*.

CDC20 forms a complex with APC/C and plays a key role in cell cycle spindle checkpoint and metaphase-to-anaphase transition. DNA damage signal has been reported to dramatically suppress the transcription of *CDC20* (Banerjee et al., 2009), and the molecular mechanism for this DNA damage-mediated *CDC20* transcription repression is not clearly understood. The hotspot mutation targeted site reported in this study can mediate the transcriptional repression of *CDC20* induced by DNA damage, and this could be one of the physiological functions of this hotspot mutation targeted DNA site.

Here a noncoding driving mutation analysis framework was developed, which focused on clustered noncoding mutations with potential functional consequence in protein factor binding. This analysis method has implications for the further development of function-based noncoding driver identification pipelines. In addition, recurrent noncoding mutation hotspots were identified in *CDC20* gene promoter; these mutations lead to increased transcription of *CDC20*, which is known to be up-regulated in various cancers and might directly stimulate cancer progression.

Limitations of the study

The functions of the identified noncoding mutations are evaluated through luciferase reporter assay in this study. The physiological function of these noncoding mutations need to be validated using additional methods, such as generating mutation knockin cell line or knockin animal model. Our *in vitro* experiments suggest that *CDC20* promoter hotspot mutations stimulate *CDC20* transcription, whereas in available human cancer samples with gene expression data, the *CDC20* expression difference between promoter mutated and unmutated samples does not reach statistical significance and more samples are required to fully demonstrate the physiological function of these *CDC20* promoter hotspot mutations in human cancer.

Resource availability

Lead contact

Further information and requests for resources and reagents should be directed to and will be fulfilled by the lead contact, Dr. Xue-Song Liu (liuxs@shanghaitech.edu.cn).

Materials availability

All unique reagents generated in this study are available from the lead contact without restriction.

Data and code availability

All mutation data used in this analysis were downloaded from ICGC data portal (https://dcc.icgc.org/). Conservation status data can be downloaded from http://hgdownload.soe.ucsc.edu/goldenPath/hg19/phastCons100way/hg19.100way.phastCons.bw. Replication timing data can be downloaded from: http://genome.ucsc.edu/cgi-bin/hgTrackUi?hgsid=686007785_bZhX09eqxKrp5MaaX8giOIZEMx14&c=chr8&g=wgEncodeUwRepliSeq. Mappability data can be downloaded from http://hgdownload.soe.ucsc.edu/goldenPath/hg19/encodeDCC/wgEncodeMapability/wgEncodeCrgMapabilityAlign24mer.bigWig. GC content data can be downloaded from http://hgdownload.soe.ucsc.edu/goldenPath/hg19/gc5Base/hg19.gc5Base.txt.gz. TFBS data can be downloaded from http://hgdownload.cse.ucsc.edu/goldenPath/hg19/encodeDCC/wgEncodeRegTfbsClustered/wgEncodeRegTfbsClusteredWithCellsV3.bed.gz. Data for epigenetic features can be downloaded from https://egg2.wustl.edu/roadmap/data/byFileType/peaks/consolidated/broadPeak/. 1000 Genomes Project phase I data can be downloaded from http://www.internationalgenome.org/data/. All the codes used to reproduce analysis results are freely available at https://github.com/XSLiuLab/Noncoding-code-2020.

METHODS

All methods can be found in the accompanying transparent methods supplemental file.

SUPPLEMENTAL INFORMATION

Supplemental information can be found online at https://doi.org/10.1016/j.isci.2021.102285.

ACKNOWLEDGMENTS

We thank the contributors and the organizers of ICGC datasets. This study has been approved by the ICGCDACO with the approval number: DACO-1068559. We thank Raymond Shuter for editing the text. We thank ShanghaiTech University High Performance Computing Public Service Platform for computing services. We thank Liye Zhang of ShanghaiTech for critical comments and helpful discussion. This work was supported in part by The National Natural Science Foundation of China (31771373) and startup funding from ShanghaiTech University.

AUTHOR CONTRIBUTIONS

Z.H. and J.Z. performed the experiments in cell lines; T.W., S.W., J.Z. collected the ICGC data and performed the programming and statistical analysis; T.W., X.S., Z.T., X.Z., H.L., and K.W. participated in critical project discussions; Z.H., T.W., S.W., J.Z., and X.-S.L. analyzed and interpreted the data; X.-S.L. designed, supervised the study and wrote the manuscript.

DECLARATION OF INTERESTS

The authors declare no competing interests.

Received: June 23, 2020
Revised: February 3, 2021
Accepted: March 4, 2021
Published: April 23, 2021

REFERENCES

Alexandrov, L.B., Nik-Zainal, S., Wedge, D.C., Aparicio, S.A., Behjati, S., Biankin, A.V., Bignell, G.R., Bolli, N., Borg, A., Borresen-Dale, A.L., et al. (2013). Signatures of mutational processes in human cancer. Nature *500*, 415–421.

Banerjee, T., Nath, S., and Roychoudhury, S. (2009). DNA damage induced p53downregulatesCdc20 by direct binding to its promoter causing chromatin remodeling. Nucleic Acids Res. *37*, 2688–2698.

Bell, R.J., Rube, H.T., Kreig, A., Mancini, A., Fouse, S.D., Nagarajan, R.P., Choi, S., Hong, C., He, D., Pekmezci, M., et al. (2015). Cancer. The transcription factor GABP selectively binds and activates the mutant TERT promoter in cancer. Science *348*, 1036–1039.

Chang, D.Z., Ma, Y., Ji, B., Liu, Y., Hwu, P., Abbruzzese, J.L., Logsdon, C., and Wang, H. (2012). Increased CDC20 expression is associated with pancreatic ductal adenocarcinoma differentiation and progression. J. Hematol. Oncol. *5*, 15.

Consortium, E.P. (2012). An integrated encyclopedia of DNA elements in the human genome. Nature *489*, 57–74.

Denisova, E., Heidenreich, B., Nagore, E., Rachakonda, P.S., Hosen, I., Akrap, I., Traves, V., Garcia-Casado, Z., Lopez-Guerrero, J.A., Requena, C., et al. (2015). Frequent DPH3 promoter mutations in skin cancers. Oncotarget *6*, 35922–35930.

Fredriksson, N.J., Elliott, K., Filges, S., Van den Eynden, J., Stahlberg, A., and Larsson, E. (2017). Recurrent promoter mutations in melanoma are defined by an extended context-specific mutational signature. PLoS Genet. *13*, e1006773.

Fredriksson, N.J., Ny, L., Nilsson, J.A., and Larsson, E. (2014). Systematic analysis of noncoding somatic mutations and gene expression alterations across 14 tumor types. Nat. Genet. *46*, 1258–1263.

Fujimoto, A., Furuta, M., Totoki, Y., Tsunoda, T., Kato, M., Shiraishi, Y., Tanaka, H., Taniguchi, H., Kawakami, Y., Ueno, M., et al. (2016). Whole-genome mutational landscape and characterization of noncoding and structural mutations in liver cancer. Nat. Genet. *48*, 500.

Gayyed, M.F., El-Maqsoud, N.M., Tawfiek, E.R., El Gelany, S.A., and Rahman, M.F. (2016). A comprehensive analysis of CDC20 overexpression in common malignant tumors from multiple organs: Its correlation with tumor grade and stage. Tumour Biol. *37*, 749–762.

Hartwell, L.H., Culotti, J., and Reid, B. (1970). Genetic control of the cell-division cycle in yeast. I. Detection of mutants. Proc. Natl. Acad. Sci. U S A *66*, 352–359.

Hartwell, L.H., Mortimer, R.K., Culotti, J., and Culotti, M. (1973). Genetic control of the cell division cycle in yeast: V. Genetic analysis of cdcmutants. Genetics *74*, 267–286.

Horn, S., Figl, A., Rachakonda, P.S., Fischer, C., Sucker, A., Gast, A., Kadel, S., Moll, I., Nagore, E., Hemminki, K., et al. (2013). TERT promoter mutations in familial and sporadic melanoma. Science *339*, 959–961.

Huang, F.W., Hodis, E., Xu, M.J., Kryukov, G.V., Chin, L., and Garraway, L.A. (2013). Highly recurrent TERT promoter mutations in human melanoma. Science *339*, 957–959.

Huang, H.C., Shi, J., Orth, J.D., and Mitchison, T.J. (2009). Evidence that mitotic exit is a better cancer therapeutic target than spindle assembly. Cancer Cell *16*, 347–358.

Jiang, J., Thyagarajan-Sahu, A., Krchnak, V., Jedinak, A., Sandusky, G.E., and Sliva, D. (2012). NAHA, a novel hydroxamic acid-derivative, inhibits growth and angiogenesis of breast cancer in vitro and in vivo. PLoS One *7*, e34283.

Kim, Y., Choi, J.W., Lee, J.H., and Kim, Y.S. (2014). MAD2 and CDC20 are upregulated in high-grade squamous intraepithelial lesions and squamous cell carcinomas of the uterine cervix. Int. J. Gynecol. Pathol. *33*, 517–523.

King, R.W., Peters, J.M., Tugendreich, S., Rolfe, M., Hieter, P., and Kirschner, M.W. (1995). A 20S complex containing CDC27 and CDC16 catalyzes the mitosis-specific conjugation of ubiquitin to cyclin B. Cell *81*, 279–288.

Lochovsky, L., Zhang, J., Fu, Y., Khurana, E., and Gerstein, M. (2015). LARVA: An integrative framework for large-scale analysis of recurrent variants in noncoding annotations. Nucleic Acids Res. *43*, 8123–8134.

Majumder, P., Bhunia, S., Bhattacharyya, J., and Chaudhuri, A. (2014). Inhibiting tumor growth by targeting liposomally encapsulated CDC20siRNA to tumor vasculature: Therapeutic RNA interference. J. Control. Release *180*, 100–108.

Mao, P., Brown, A.J., Esaki, S., Lockwood, S., Poon, G.M.K., Smerdon, M.J., Roberts, S.A., and Wyrick, J.J. (2018). ETS transcription factors induce a unique UV damage signature that drives recurrent mutagenesis in melanoma. Nat. Commun. *9*, 2626.

Maurano, M.T., Humbert, R., Rynes, E., Thurman, R.E., Haugen, E., Wang, H., Reynolds, A.P., Sandstrom, R., Qu, H., Brody, J., et al. (2012). Systematic localization of common disease-associated variation in regulatory DNA. Science *337*, 1190–1195.

Melton, C., Reuter, J.A., Spacek, D.V., and Snyder, M. (2015). Recurrent somatic mutations in regulatory regions of human cancer genomes. Nat. Genet. *47*, 710–716.

Mukherjee, A., Bhattacharyya, J., Sagar, M.V., and Chaudhuri, A. (2013). Liposomally encapsulated CDC20siRNA inhibits both solid melanoma tumor growth and spontaneous growth of intravenously injected melanoma cells on mouse lung. Drug Deliv. Transl. Res. *3*, 224–234.

Pesin, J.A., and Orr-Weaver, T.L. (2008). Regulation of APC/C activators in mitosis and meiosis. Annu. Rev.Cell Dev. Biol. *24*, 475–499.

Rheinbay, E., Nielsen, M.M., Abascal, F., Wala, J.A., Shapira, O., Tiao, G., Hornshoj, H., Hess, J.M., Juul, R.I., Lin, Z., et al. (2020). Analyses of non-coding somatic drivers in 2,658 cancer whole genomes. Nature *578*, 102–111.

Rheinbay, E., Parasuraman, P., Grimsby, J., Tiao, G., Engreitz, J.M., Kim, J., Lawrence, M.S., Taylor-Weiner, A., Rodriguez-Cuevas, S., Rosenberg, M., et al. (2017). Recurrent and functional regulatory mutations in breast cancer. Nature *547*, 55–60.

Schuster-Bockler, B., and Lehner, B. (2012). Chromatin organization is a major influence on regional mutation rates in human cancer cells. Nature *488*, 504–507.

Sizemore, G.M., Pitarresi, J.R., Balakrishnan, S., and Ostrowski, M.C. (2017). The ETS family of oncogenic transcription factors in solid tumours. Nat. Rev. Cancer *17*, 337–351.

Sudakin, V., Ganoth, D., Dahan, A., Heller, H., Hershko, J., Luca, F.C., Ruderman, J.V., and Hershko, A. (1995). The cyclosome, a large complex containing cyclin-selective ubiquitin ligase activity, targets cyclins for destruction at the end of mitosis. Mol. Biol. Cell *6*, 185–197.

Wang, Z., Wan, L., Zhong, J., Inuzuka, H., Liu, P., Sarkar, F.H., and Wei, W. (2013). Cdc20: A potential novel therapeutic target for cancer treatment. Curr. Pharm. Des. *19*, 3210–3214.

Weinhold, N., Jacobsen, A., Schultz, N., Sander, C., and Lee, W. (2014). Genome-wide analysis of noncoding regulatory mutations in cancer. Nat. Genet. *46*, 1160–1165.

Zeng, X., Sigoillot, F., Gaur, S., Choi, S., Pfaff, K.L., Oh, D.C., Hathaway, N., Dimova, N., Cuny, G.D., and King, R.W. (2010). Pharmacologic inhibition of the anaphase-promoting complex induces a spindle checkpoint-dependent mitotic arrest in the absence of spindle damage. Cancer Cell *18*, 382–395.

Zhang, W., Bojorquez-Gomez, A., Velez, D.O., Xu, G., Sanchez, K.S., Shen, J.P., Chen, K., Licon, K., Melton, C., Olson, K.M., et al. (2018). A global transcriptional network connecting noncoding mutations to changes in tumor gene expression. Nat. Genet. *50*, 613–620.

iScience, Volume *24*

Supplemental information

Pan-cancer noncoding genomic analysis identifies functional *CDC20* promoter mutation hotspots

Zaoke He, Tao Wu, Shixiang Wang, Jing Zhang, Xiaoqin Sun, Ziyu Tao, Xiangyu Zhao, Huimin Li, Kai Wu, and Xue-Song Liu

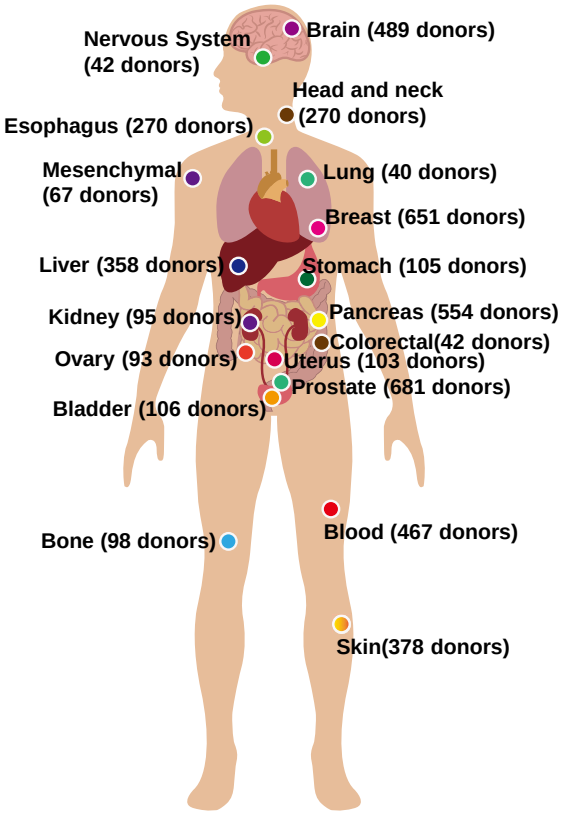

Figure S1. Summary of pan-cancer noncoding analysis data, Related to Figure 1. Number of tumor samples by disease types.

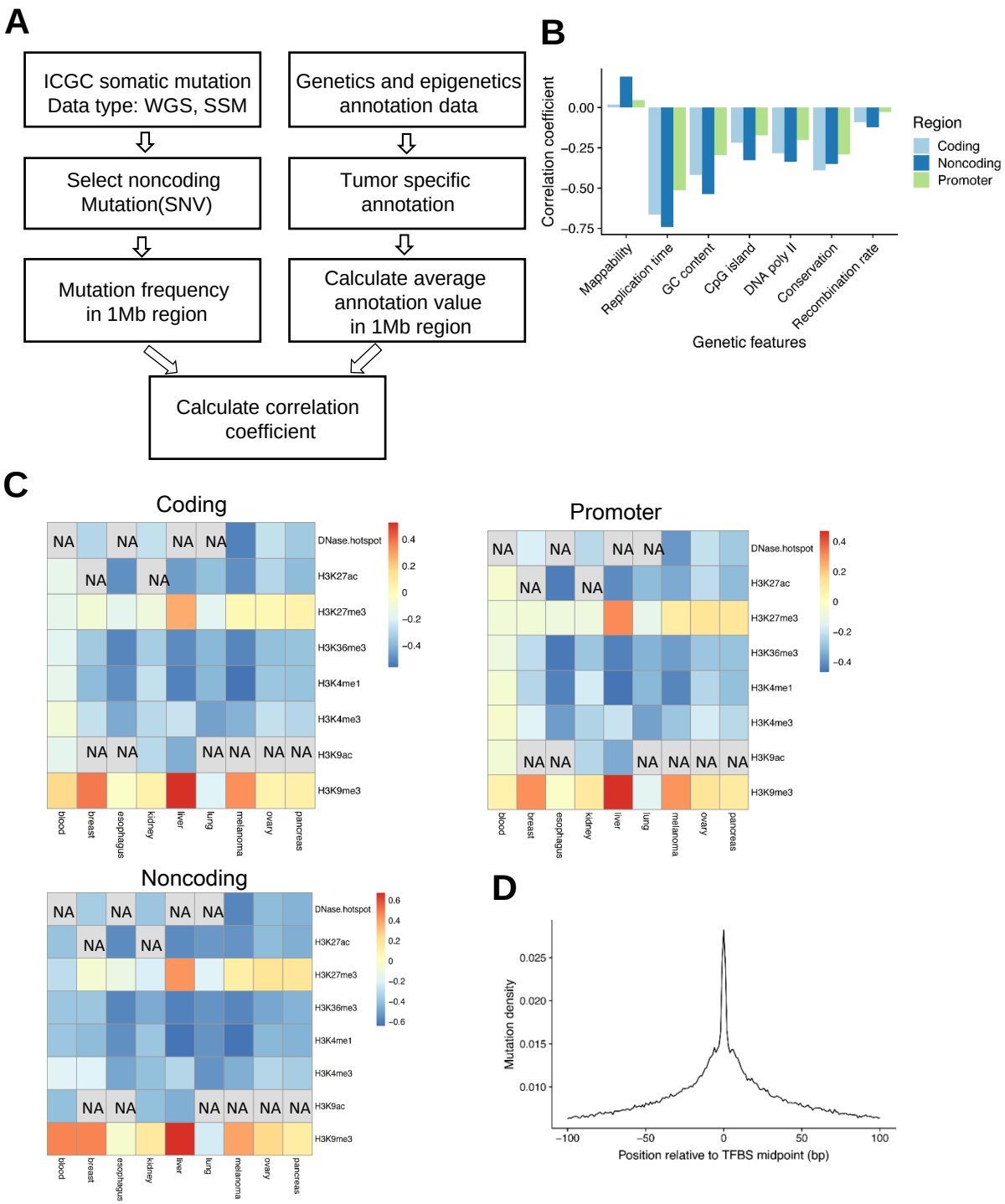

Figure S2. Correlations between coding, noncoding mutation rates and genetic or epigenetic features, Related to Figure 1. (A) Workflow for the correlation analysis between background mutation rates and genetic or epigenetic features. (B) Correlations between genetic features and coding, noncoding, promoter mutation rates. (C) Pearson correlations between epigenetic features and mutation rates in coding, noncoding and promoter regions. (D) Mutation density surrounding TFBS from 4856 ICGC cancer samples.

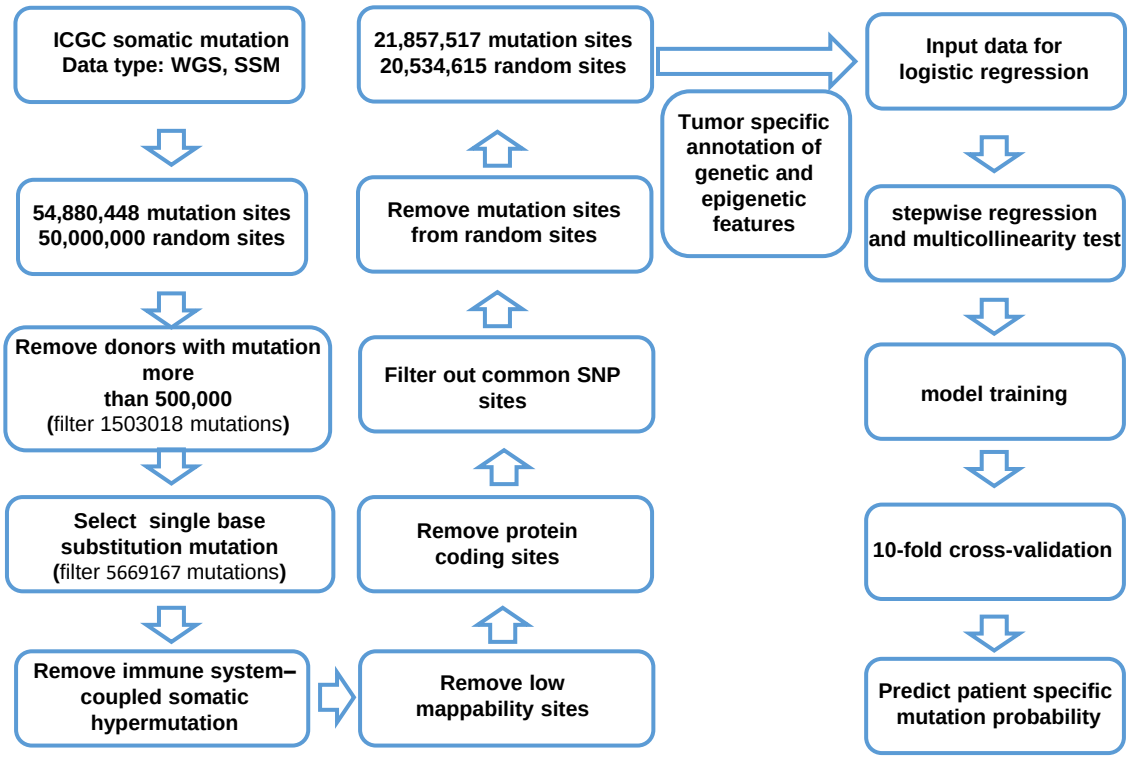

Figure S3. Workflow for the calculation of patient-specific background mutation probability, Related to Figure 1. Flowchart of procedures for calculating patient-specific background mutation probability for noncoding sites using logistic regression model incorporating genetic and epigenetic features of each noncoding site.

Mutation Cluster Region	Nearest Gene	Frequency	P value	Adjust p value
chr5:1295223-1295233	TERT	55	1.93179E-14	6.04843E-10
chr3:16306499-16306510	OXNAD1	39	2.20934E-14	6.91746E-10
chr3:16306499-16306510	DPH3	39	2.20934E-14	6.91746E-10
chr5:1295245-1295255	TERT	39	3.67484E-14	1.15059E-09
chr3:101280665-101280676	TRMT10C	34	1.58762E-14	4.97083E-10
chr8:56987136-56987146	RPS20	27	7.99361E-15	2.5028E-10
chr1:43824520-43824534	CDC20	27	1.4877E-14	4.65799E-10
chr11:47448140-47448154	PSMC3	27	3.66374E-14	1.14712E-09
chr19:17970677-17970687	RPL18A	25	2.27596E-14	7.12602E-10
chr13:41345341-41345351	MRPS31	23	5.55112E-15	1.73805E-10
chr1:155904245-155904255	KIAA0907	23	1.05471E-14	3.3023E-10
chr10:105156311-105156322	PDCD11	22	5.88418E-15	1.84234E-10
chr10:105156311-105156322	USMG5	22	5.88418E-15	1.84234E-10
chr2:32390899-32390910	SLC30A6	21	1.74305E-14	5.45749E-10
chr1:179846979-179846990	TOR1AIP1	20	1.0103E-14	3.16326E-10
chr1:179846979-179846990	TOR1AIP2	20	1.0103E-14	3.16326E-10
chr1:100598548-100598558	TRMT13	20	1.08802E-14	3.40659E-10
chr1:100598548-100598558	SASS6	20	1.08802E-14	3.40659E-10
chr19:7459935-7459946	ARHGEF18	20	1.54321E-14	4.83179E-10
chr9:131038408-131038419	GOLGA2	20	1.82077E-14	5.70082E-10
chr2:70056746-70056757	GMCL1	19	3.44169E-15	1.07759E-10
chr9:35658036-35658047	CCDC107	19	2.14273E-14	6.70889E-10
chr11:98886777-98886796	CNTN5	18	6.99441E-15	2.18995E-10
chr2:26101483-26101494	ASXL2	18	1.25455E-14	3.928E-10
chr22:44208288-44208298	EFCAB6	17	1.24345E-14	3.89324E-10
chr2:176991924-176991943	HOXD8	17	1.25455E-14	3.928E-10
chr12:54582884-54582895	SMUG1	17	1.76525E-14	5.52701E-10
chr19:17970555-17970565	RPL18A	16	6.43929E-15	2.01614E-10
chr15:90931378-90931388	IQGAP1	16	6.66134E-15	2.08566E-10
chr8:114450090-114450103	CSMD3	16	1.12133E-14	3.51087E-10
chr17:7338578-7338588	TMEM102	16	1.31006E-14	4.10181E-10
chr17:7338578-7338588	FGF11	16	1.31006E-14	4.10181E-10
chr6:149867280-149867291	PPIL4	15	6.77236E-15	2.12043E-10
chr12:498771-498781	KDM5A	15	8.77076E-15	2.74613E-10
chr22:31556116-31556126	RNF185	15	8.77076E-15	2.74613E-10
chr1:153963222-153963232	RPS27	15	1.05471E-14	3.3023E-10
chr1:153963222-153963232	RAB13	15	1.05471E-14	3.3023E-10
chr16:27561360-27561371	KIAA0556	14	5.44009E-15	1.70329E-10
chr16:27561360-27561371	GTF3C1	14	5.44009E-15	1.70329E-10
chr1:25559058-25559069	SYF2	14	5.77316E-15	1.80758E-10
chr13:60738136-60738147	DIAPH3	14	8.10463E-15	2.53756E-10
chr22:35795970-35795981	MCM5	14	8.32667E-15	2.60708E-10
chr2:198318139-198318149	COQ10B	14	8.88178E-15	2.78089E-10
chr16:67260975-67260988	TMEM208	14	1.14353E-14	3.58039E-10
chr16:67260975-67260988	AC040160.1	14	1.14353E-14	3.58039E-10
chr16:67260975-67260988	LRRC29	14	1.14353E-14	3.58039E-10
chr17:1588271-1588281	PRPF8	14	1.37668E-14	4.31037E-10
chr11:73309651-73309662	FAM168A	13	6.32827E-15	1.98138E-10
chr10:18940596-18940606	NSUN6	13	6.88338E-15	2.15519E-10

Figure S4. List of significantly mutated noncoding regions, Related to Figure 2. Eleven base pair Noncoding DNA regions are first ranked based on mutation probability, and top 50 ($-\text{Log}_{10}$ (P Value)) noncoding regions are further ranked based on mutation frequency. Nearest genes to each noncoding regions are also shown.

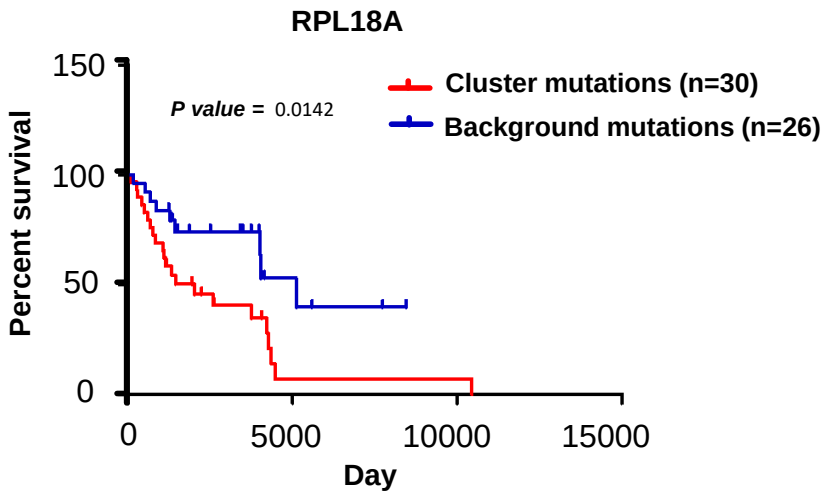

Figure S5. Kaplan–Meier overall survival curves of melanoma patients with indicated *RPL18A* promoter mutations or other mutations in the background, Related to Figure 2. n=30 for melanoma patients with clustered *RPL18A* promoter mutations (Chr19: C17970682T and G17970560A) and n=26 for melanoma patients with other mutations in the background region. Log-rank (Mantel-Cox) test *P* value is shown.

7bp window

Mutation Cluster Region	gene_name	count	adj_p_val
chr5:1295225-1295231	TERT	55	3.13E-10
chr3:16306501-16306508	OXNAD1	39	5.15E-10
chr3:16306501-16306508	DPH3	39	5.15E-10
chr5:1295247-1295253	TERT	38	3.06E-10
chr3:101280667-101280674	TRMT10C	34	7E-10
chr11:47448142-47448152	PSMC3	27	7.94E-10
chr1:43824522-43824532	CDC20	26	1.74E-10
chr8:56987138-56987144	RPS20	26	1.21E-09
chr19:17970679-17970685	RPL18A	25	7.56E-10
chr13:41345343-41345349	MRPS31	23	7E-304
chr1:155904247-155904253	KIAA0907	23	1.03E-09
chr10:105156313-105156320	PDCD11	22	1.02E-09
chr10:105156313-105156320	USMG5	22	1.02E-09
chr2:32390901-32390908	SLC30A6	20	1.21E-09
chr1:100598550-100598556	TRMT13	19	5.36E-10

9bp window

Mutation Cluster Region	gene_name	count	adj_p_val
chr5:1295224-1295232	TERT	55	6.26E-11
chr5:1295246-1295254	TERT	39	4.38E-10
chr3:16306500-16306509	OXNAD1	39	6.89E-10
chr3:16306500-16306509	DPH3	39	6.89E-10
chr3:101280666-101280675	TRMT10C	34	8.21E-10
chr11:47448141-47448153	PSMC3	27	1.12E-09
chr1:43824521-43824533	CDC20	26	4.87E-10
chr8:56987137-56987145	RPS20	26	1.16E-09
chr19:17970678-17970686	RPL18A	25	6.99E-10
chr13:41345342-41345350	MRPS31	23	1.04E-11
chr1:155904246-155904254	KIAA0907	23	9.98E-10
chr10:105156312-105156321	PDCD11	22	8.73E-10
chr10:105156312-105156321	USMG5	22	8.73E-10
chr2:32390900-32390909	SLC30A6	21	1.12E-09
chr1:100598549-100598557	TRMT13	20	4.7E-10

13bp window

Mutation Cluster Region	gene_name	count	adj_p_val
chr5:1295222-1295234	TERT	55	2.81E-10
chr5:1295244-1295256	TERT	39	3.58E-10
chr3:16306498-16306511	OXNAD1	39	8.09E-10
chr3:16306498-16306511	DPH3	39	8.09E-10
chr3:101280664-101280677	TRMT10C	34	8.89E-10
chr1:43824519-43824535	CDC20	27	5.97E-10
chr11:47448139-47448155	PSMC3	27	9.31E-10
chr8:56987135-56987147	RPS20	27	1.11E-09
chr19:17970676-17970688	RPL18A	25	1.07E-09
chr13:41345340-41345352	MRPS31	23	1.04E-11
chr1:155904244-155904256	KIAA0907	23	1.09E-09
chr10:105156310-105156323	PDCD11	22	8.54E-10
chr10:105156310-105156323	USMG5	22	8.54E-10
chr2:32390898-32390911	SLC30A6	21	1.06E-09
chr9:35658035-35658048	CCDC107	20	2.95E-10

15bp window

Mutation Cluster Region	gene_name	count	adj_p_val
chr5:1295221-1295235	TERT	55	2.67E-10
chr5:1295243-1295257	TERT	39	5.76E-10
chr3:16306497-16306512	OXNAD1	39	7.85E-10
chr3:16306497-16306512	DPH3	39	7.85E-10
chr3:101280663-101280678	TRMT10C	34	8.65E-10
chr8:56987134-56987148	RPS20	30	1.14E-09
chr1:43824518-43824536	CDC20	27	4.13E-10
chr11:47448138-47448156	PSMC3	27	1.01E-09
chr19:17970675-17970689	RPL18A	25	9.06E-10
chr13:41345339-41345353	MRPS31	23	7E-304
chr1:155904243-155904257	KIAA0907	23	7.85E-10
chr10:105156309-105156324	PDCD11	22	1.03E-09
chr10:105156309-105156324	USMG5	22	1.03E-09
chr11:98886775-98886798	CNTN5	21	6.77E-10
chr2:32390897-32390912	SLC30A6	21	9.41E-10

17bp window

Mutation Cluster Region	gene_name	count	adj_p_val
chr5:1295220-1295236	TERT	55	2.67E-10
chr5:1295242-1295258	TERT	39	5E-10
chr3:16306496-16306513	OXNAD1	39	7.98E-10
chr3:16306496-16306513	DPH3	39	7.98E-10
chr3:101280662-101280679	TRMT10C	34	9.99E-10
chr8:56987133-56987149	RPS20	30	1.15E-09
chr1:43824517-43824537	CDC20	28	3.75E-10
chr11:47448137-47448157	PSMC3	27	9.86E-10
chr19:17970674-17970690	RPL18A	25	1.13E-09
chr1:155904242-155904258	KIAA0907	24	1.01E-09
chr13:41345338-41345354	MRPS31	23	3.82E-11
chr9:35658033-35658050	CCDC107	22	5.14E-10
chr10:105156308-105156325	PDCD11	22	1.09E-09
chr10:105156308-105156325	USMG5	22	1.09E-09
chr11:98886774-98886799	CNTN5	21	4.65E-10

21bp window

Mutation Cluster Region	gene_name	count	adj_p_val
chr5:1295218-1295238	TERT	55	4.44E-10
chr5:1295240-1295260	TERT	39	7.49E-10
chr3:16306494-16306515	OXNAD1	39	9.01E-10
chr3:16306494-16306515	DPH3	39	9.01E-10
chr3:101280660-101280681	TRMT10C	34	9.74E-10
chr8:56987131-56987151	RPS20	30	1.06E-09
chr1:43824515-43824539	CDC20	28	6.07E-10
chr16:67260952-67261010	TMEM208	27	8.11E-10
chr16:67260952-67261010	AC040160.1	27	8.11E-10
chr16:67260952-67261010	LRRC29	27	8.11E-10
chr1:153963184-153963237	RPS27	27	9.15E-10
chr1:153963184-153963237	RAB13	27	9.15E-10
chr11:47448135-47448159	PSMC3	27	1.17E-09
chr19:17970672-17970692	RPL18A	25	9.5E-10
chr1:155904240-155904260	KIAA0907	24	9.46E-10

Figure S6. List of significantly mutated noncoding regions calculated with different size of window (From 7bp to 21bp window), Related to Figure 2.
Noncoding DNA regions are first ranked based on mutation probability, and top 50 ($-\text{Log}_{10}$ (P Value)) noncoding regions are further ranked based on mutation frequency.

Regions	gene_name	count	p_val	adj_p_val
chr3:46780065-46780075	PRSS46	9	1.9873E-14	1.3911E-11
chr3:167375318-167375328	WDR49	6	1.5654E-14	1.0958E-11
chr8:42399654-42399664	SLC20A2	6	2.7756E-14	1.9429E-11
chr3:11765471-11765481	VGLL4	5	1.5654E-14	1.0958E-11
chr1:156859617-156859627	PEAR1	5	2.0095E-14	1.4067E-11
chr3:11034286-11034296	SLC6A1	5	2.6312E-14	1.8419E-11
chr14:21078826-21078836	RNASE11	5	4.4368E-12	3.1057E-09
chr14:21078826-21078836	RNASE11	5	4.4368E-12	3.1057E-09
chr12:10162489-10162499	CLEC12B	5	1.1796E-09	8.2569E-07
chr11:48388090-48388100	OR4C5	4	3.0198E-14	2.1139E-11
chr13:106115297-106115307	DAOA	4	6.2506E-14	4.3754E-11
chr11:118174980-118174990	CD3E	4	5.258E-13	3.6806E-10
chr20:63544-63554	DEFB125	4	7.9448E-13	5.5613E-10
chr19:52040086-52040096	SIGLEC6	4	1.5451E-12	1.0816E-09
chr19:48763863-48763873	CARD8	4	3.4791E-12	2.4354E-09
chr10:124765924-124765934	ACADSB	4	1.3451E-11	9.4155E-09

Figure S7. List of significantly mutated noncoding indels calculated with 11bp window, Related to Figure 2. Noncoding DNA regions with clustered indels in 11bp window are first ranked based on indel probability, and top 50 ($-\text{Log}_{10}$ (P Value)) noncoding regions are further ranked based on the frequency of indel.

Mutation Cluster Region	gene_name	sequenceType	count	p_val	adj_p_val
chr5:1295223-1295233	TERT	promoter	55	1.07E-14	3.34E-10
chr1:203275149-203275166	BTG2	intron	41	1.14E-14	3.58E-10
chr5:1295245-1295255	TERT	promoter	39	1.12E-14	3.51E-10
chr3:16306499-16306510	OXNAD1	promoter	39	2.64E-14	8.27E-10
chr3:16306499-16306510	DPH3	promoter	39	2.64E-14	8.27E-10
chr19:10340883-10340911	S1PR2	intron	36	1.47E-14	4.59E-10
chr1:203275100-203275113	BTG2	intron	36	2.25E-14	7.06E-10
chr1:203274969-203274988	BTG2	intron	34	1.09E-14	3.41E-10
chr3:101280665-101280676	TRMT10C	promoter	34	2.96E-14	9.28E-10
chr1:203275555-203275578	BTG2	intron	33	2.08E-14	6.5E-10
chr9:37026307-37026318	PAX5	intron	28	1.45E-14	4.55E-10
chr2:136875308-136875336	CXCR4	intron	27	1.17E-14	3.65E-10
chr1:43824520-43824534	CDC20	promoter	27	1.2E-14	3.75E-10
chr11:47448140-47448154	PSMC3	promoter	27	3.66E-14	1.15E-09
chr8:56987136-56987146	RPS20	5_utr	27	3.86E-14	1.21E-09
chr8:56987136-56987146	RPS20	promoter	27	3.86E-14	1.21E-09
chr1:240636863-240636873	FMN2	intron	26	8.66E-15	2.71E-10
chr16:10973681-10973696	CIITA	intron	25	1.51E-14	4.73E-10
chr1:203275173-203275197	BTG2	intron	25	1.89E-14	5.91E-10
chr19:17970677-17970687	RPL18A	promoter	25	2.78E-14	8.69E-10
chr19:17970677-17970687	RPL18A	5_utr	25	2.78E-14	8.69E-10
chr10:115511585-115511598	PLEKHS1	intron	24	8.55E-15	2.68E-10
chr13:41345341-41345351	MRPS31	5_utr	23	0	7E-304
chr13:41345341-41345351	MRPS31	promoter	23	0	7E-304
chr1:999995-1000005	BC033949	intron	23	0	7E-304
chr1:155904245-155904255	KIAA0907	promoter	23	3.06E-14	9.59E-10
chr5:22578492-22578502	CDH12	intron	23	3.18E-14	9.94E-10
chr1:203275075-203275090	BTG2	intron	22	8.88E-15	2.78E-10
chr6:91005801-91005819	BACH2	intron	22	1.28E-14	4E-10
chr2:136875033-136875051	CXCR4	intron	22	1.78E-14	5.56E-10
chr9:37025356-37025366	PAX5	intron	22	2E-14	6.26E-10
chr1:203274951-203274966	BTG2	intron	22	2.08E-14	6.5E-10
chr6:6307789-6307799	F13A1	intron	22	2.12E-14	6.64E-10
chr2:77611356-77611366	LRRTM4	intron	22	2.24E-14	7.02E-10
chr10:105156311-105156322	PDCD11	promoter	22	2.69E-14	8.41E-10
chr10:105156311-105156322	USMG5	promoter	22	2.69E-14	8.41E-10
chr2:32390899-32390910	SLC30A6	promoter	21	3.15E-14	9.87E-10
chr2:32390899-32390910	SLC30A6	5_utr	21	3.15E-14	9.87E-10
chr7:137139140-137139152	DGKI	intron	21	3.28E-14	1.03E-09
chr1:203275118-203275140	BTG2	intron	21	3.38E-14	1.06E-09
chr6:125531722-125531734	TPD52L1	intron	20	1.14E-14	3.58E-10
chr13:33608075-33608085	KL	intron	20	1.58E-14	4.94E-10
chr9:37026725-37026736	PAX5	intron	20	1.75E-14	5.49E-10
chr8:2031625-2031656	MYOM2	intron	20	2.23E-14	6.99E-10
chr1:100598548-100598558	TRMT13	promoter	20	2.26E-14	7.09E-10
chr1:100598548-100598558	SASS6	promoter	20	2.26E-14	7.09E-10
chr1:179846979-179846990	TOR1AIP1	promoter	20	2.71E-14	8.48E-10
chr1:179846979-179846990	TOR1AIP2	promoter	20	2.71E-14	8.48E-10
chr9:131038408-131038419	GOLGA2	promoter	20	2.76E-14	8.66E-10
chr2:136874959-136874978	CXCR4	intron	20	3.29E-14	1.03E-09

Figure S8. List of significantly mutated noncoding mutations in 5'-UTR, 3'-UTR and intron regions, Related to Figure 2. Noncoding DNA regions are first ranked based on mutation probability in 11bp window, and top 50 ($-\text{Log}_{10}$(P Value)) noncoding regions are further ranked based on mutation frequency.

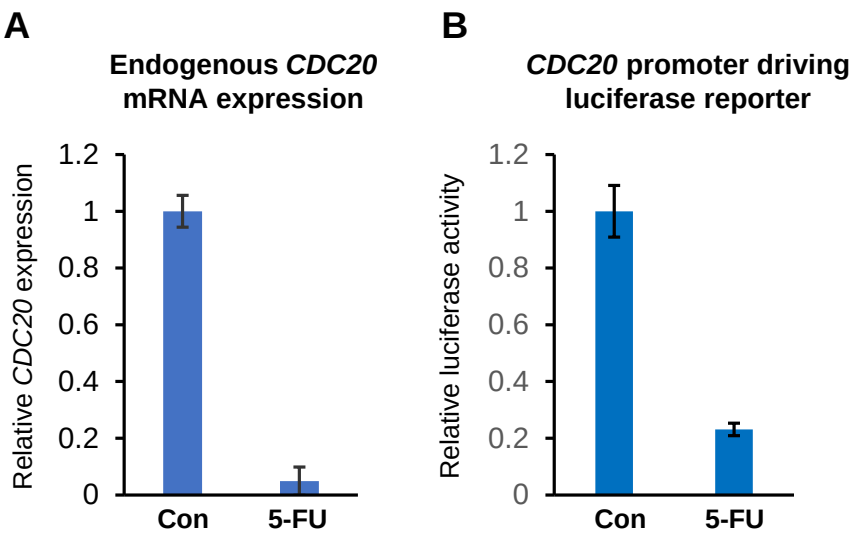

Figure S9. *CDC20* promoter driving luciferase reporter can mimic the response of human endogenous *CDC20* promoter in response to DNA damage drug, Related to Figure 4.

(A) Endogenous *CDC20* mRNA expression in response to DNA damage drug 5-FU in M14 cells. The expressions of *CDC20* mRNA were quantified by Q-PCR.

(B) Luciferase activity of cloned *CDC20* promoter-driving reporter in response to 5-FU in M14 cells. Error bars represent mean ± s.d. from three experiments.

A

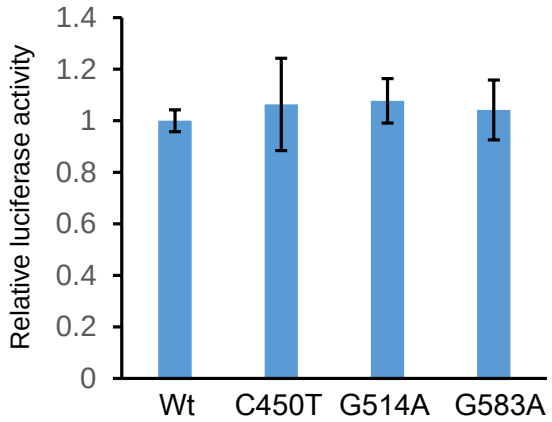

B

ATTCCCACAAACTTCTTTGTATGACCTCGGGCACATCCCTTCCCTGGGCCTCCGTTTCTCCATCTGTAAAAT
ATGGATTTGTTGTCGGGGTGGGGAGGCTGCACCACGCACAGGTTAGACTAATGGATCTCTAAGGTCCTCA
CATCTTTAAAGCCCCAAGGGGATAAGCCACAGTGCCTCCTGTAGGGCAGTCTAAGCTTATCTTCCAGATA
GGCAGGTTTGAATACCGATCCTTTTTCTTGACCTTAAGGAATTCATTCACCCTTTTCAACCTCATTTTCCCTG
TTTGTAAAACAACAGCAAACGAGACAAACACACGTTACTTCCTTTCTAGCAGGGTTCCTACCCGGCGCCAA
GCAAAAGTGGAATGTACCCTAAGTAGCTCTGGCCTTCTTCCTGCTCCCAAGCTTCCCAATTCCGTCCCCTGC
CCCGCTGCCGCCCGCGGCTCTCCTTCCCCTTCTAGGAACGGCTCAAGCGCCTTGGGCACTCCATCGGGTTC
TGCACCGAGTTCTGCATCATAAATACGACTCTCGTGTAGGATTTAAGTGTGAACTTCTGCAGGTTCTCGGA
CCCTGAAGCACCCGGGGCCAGACATTCCGAGCTCGCGGCGGTGGAAGGCACGCAAAAGGGCGAACCGA
GACGACTCCAGGACGCTGAGGCAGCGCAGGCCCCACCCGGCCCCGCCCTGCCCCGCCCTGTCCCGGCCGG
CTTTCCAGTACTAGTCCTCTGGCGC**C**(C450T)GGCTCCCAGCCCCTCTCGTACCCTTCAAATCGCGCTCCG
CCGCTAGACTCTCGTGATAGCTGA**G**(G514A)ACTTTCCCCG**G**AA**GG**CCCGCCCCCTTCGCCGGAGAG
GCCAATGGGCTAGGGCAACGGTTGCGACGGTT**G**(G583A)GATTTTGAAGGAGCCAATAGGCGCTCGG
AGCGGAGAGTTTAAGAGGCGTAAGCCAGGCGTGTTAAAGCCGGTCGGAACTGCTCCGGAGGGCACGGT
GAGAGGTGGTGGGGCTGAGCCGAGGTGGGGCCGTGGCCAGGGGGAGGGGGTGCTAGGCCGGAAGGG
GCTGCAGCCGAGGGTGGCCCTGATTTTGTGGCCGGCCAGGAGCGAAGGGGTCCCTTTCTGTCCCCTGAGC
AC

Figure S10. Random mutations in *CDC20* promoter-driving luciferase reporter did not influence luciferase activity, Related to Figure 4.

(A) Luciferase reporter assay was performed with wild-type promoter or C450T, G514A, G583A mutations in M14 cells. Error bars represent mean ± s.d. from three experiments.

(B) *CDC20* promoter sequence used for luciferase reporter assay is shown, and the locations of each mutations are labeled.

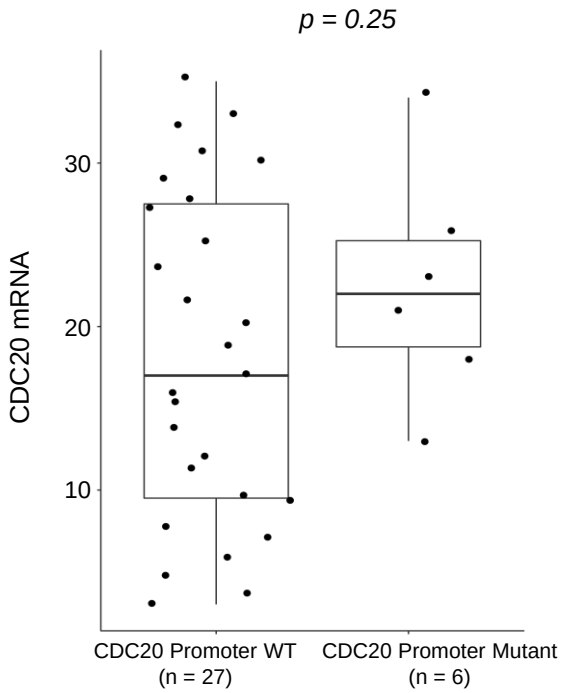

Figure S11. CDC20 mRNA levels in melanoma samples with or without the promoter hotspot mutations, Related to Figure 4. In total 6 samples with the CDC20 promoter hotspot mutations and 27 samples without the promoter hotspot mutations have gene expression data available for analysis. *P* value is calculated with unpaired, two-tailed Student's t test.

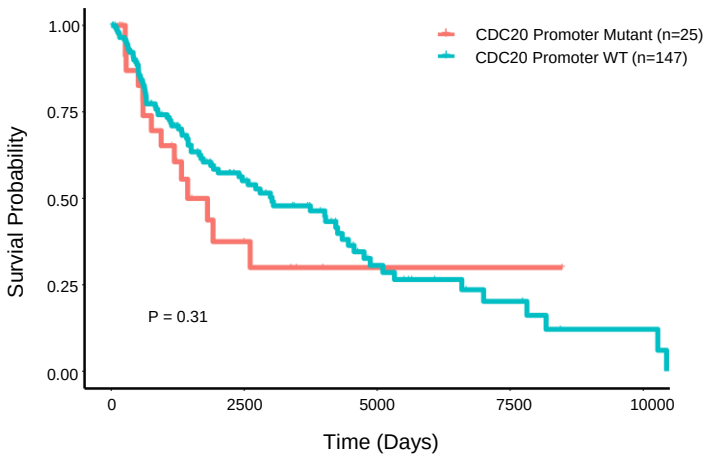

Figure S12. Kaplan–Meier overall survival curves of melanoma patients with indicated *CDC20* promoter mutations or control mutations, Related to Figure 4. n=25 for patients with clustered *CDC20* promoter mutations (including G25A, G28A, G29A and GG28/29AA), n=147 for patients without the clustered promoter mutations. Log-rank (Mantel-Cox) test *P* value is shown.

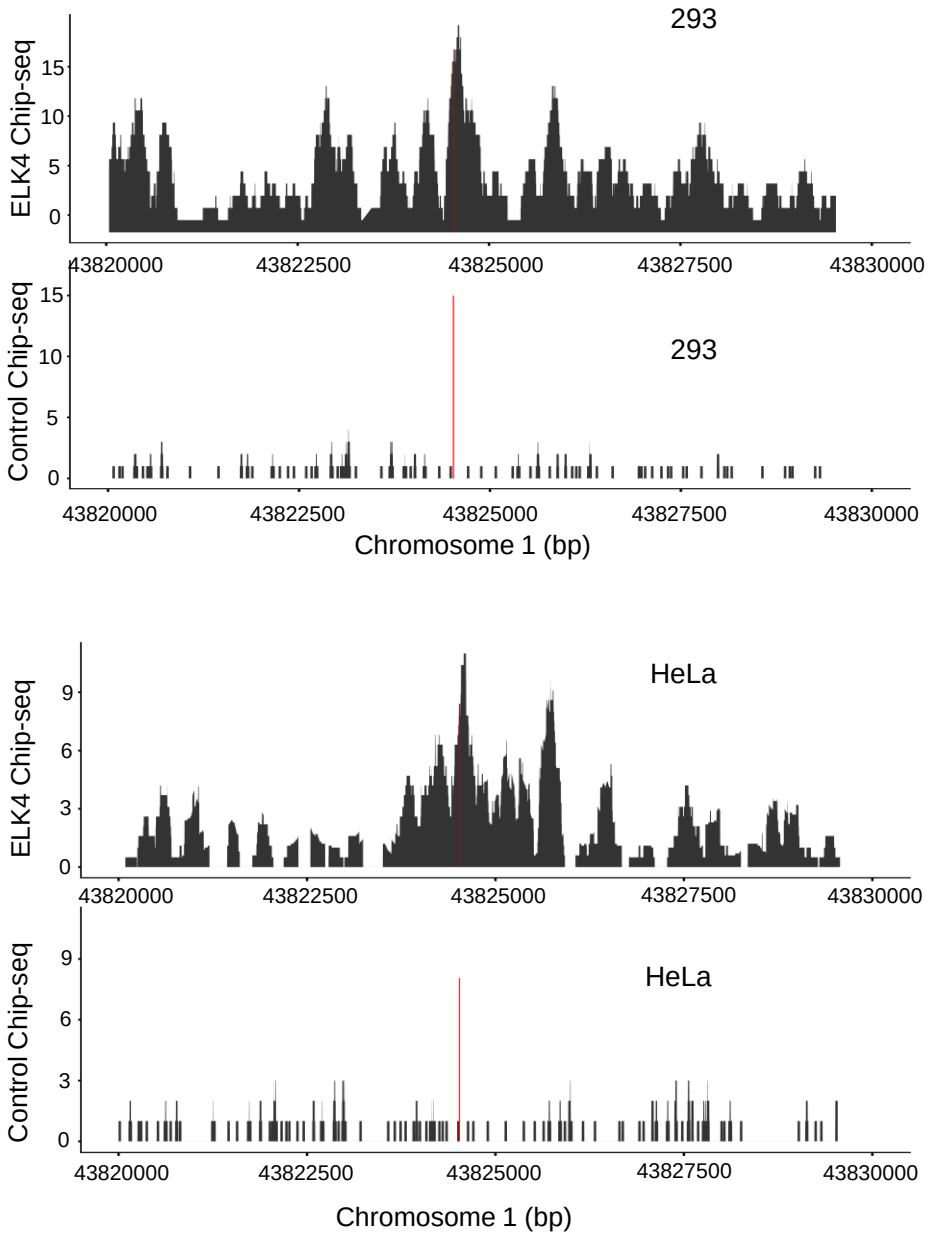

Figure S13. A zoomed out version of Figure 5B is shown, Related to Figure 5. ENCODE ELK4 and control ChIP-seq data around the hotspot mutation target sequence “GGAAGG” (marked as red line) in 293 and HeLa cells.

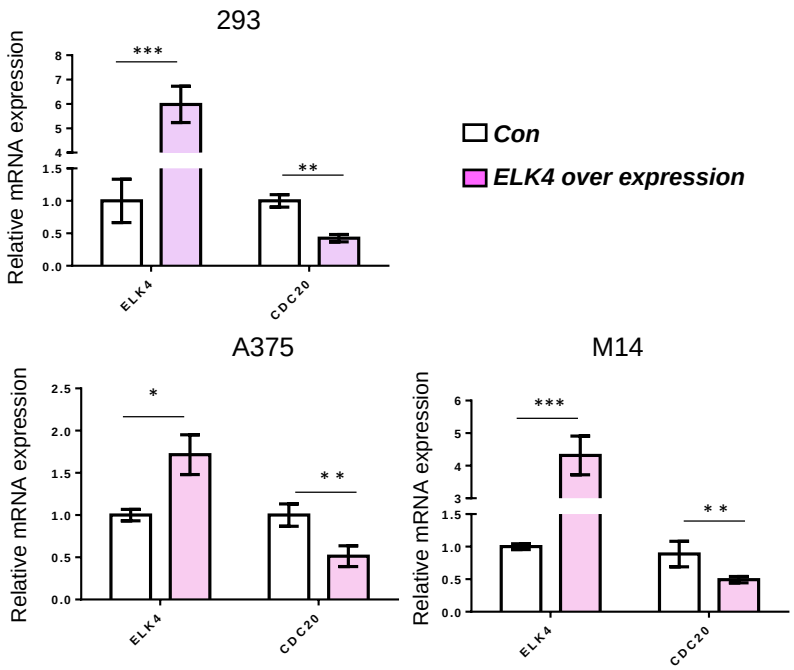

Figure S14. Overexpression of *ELK4* suppresses *CDC20* in multiple cell lines, Related to Figure 5. The expression of *ELK4* and *CDC20* mRNA were quantified by Q-PCR.

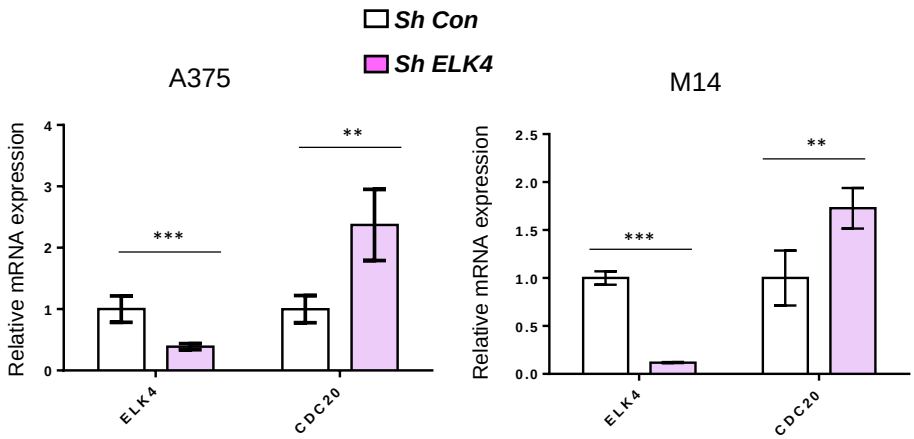

Figure S15. Knockdown of *ELK4* stimulates *CDC20* transcription in cell lines, Related to Figure 5. *ELK4* was knockdown with shRNA, the expression of *ELK4* and *CDC20* mRNA were quantified by Q-PCR.

Transparent Methods

Cancer genome data preprocessing

The reference genome used throughout this study is hg19. We downloaded cancer whole-genome sequencing (WGS) data from International Cancer Genome Consortium (ICGC) release 27. In total, there were 4,881 donors, 54,880,488 mutation sites and 59,699,855 mutations before data preprocessing. Nine samples with more than 500,000 mutations were excluded to eliminate ultra-mutated samples. We extracted mutation type "*single base substitution*" (point mutations) for analysis, and several samples without single base substitution have been removed from analysis. Common human SNP variants were removed from the cancer genome mutation datasets based on 1000 Genomes Project (Genomes Project et al., 2015). We also removed the immunoglobulin loci region according to the Ensembl (v75) annotation from further analysis to avoid bias from immune system-coupled somatic hypermutation. The final mutation data was converted to BED format for subsequent analysis. In total 4859 samples with 47,708,263 mutations are included in downstream analysis.

Genetic and epigenetic features as covariates of background mutation rates

We used a variety of annotation features to analyze background mutation rates. These features can be roughly divided into genetic features and epigenetic features. The values of genetic features are determined by the genomic DNA sequence, and are thus consistent in different tumor types. The values of epigenetic features show variations among cancer types with different tissue origins. The values of these annotation features were downloaded from UCSC genome browser database or ENCODE database, and are described as below.

Sequence context: We used the 3 base pairs nucleotide motifs centered at the mutated site (1-bp left/right flank motifs of the site). Reverse compliment pairs are combined together, in total there are 32 types of sequence contexts.

Genome mappability: This feature refer to the uniqueness of DNA sequence in mapping with reference genome. Genome mappability data was downloaded from UCSC Genome Browser.

Recombination rate: Recombination in meiosis help to expand genetic diversity. In somatic cells, DNA lesions can be repaired through recombination between homologous chromosomes. Recombination rate data was downloaded from UCSC Genome Browser.

Conservation: We used phastCons data (hg19.100way.phastCons.bw)

downloaded from UCSC genome browser to reflect the conservation status of genomic DNA. PhastCons estimates the probability that each nucleotide belongs to a conserved element, based on a phylogenetic hidden Markov model (Siepel et al., 2005).**Error! Reference source not found.**

Replication timing: We used the ENCODE replication timing data downloaded from the UCSC genome browser. The average wavelet-smoothed signals of repli-seq from 14 cell lines: BJ, GM06990, GM12801, GM12812, GM12813, GM12878, HeLa-S3, HepG2, HUVEC, IMR-90, K-562, MCF-7, NHEK and SK-N-SH were used to assess the genome-wide DNA replication timing.

GC contents: We used GC content raw data in UCSC genome browser to calculate GC content. The file hg19.gc5Base.txt.gz contains the GC content for 5bp windows across whole genome was downloaded with hgGcPercent.

CpG islands: We used UCSC Genome Browser tools to download CpG islands data. The selection criteria is “Mammal”, “Human”, “GRCH37/hg19”, “Regulation”, “CpG Islands”.

Promoters: We selected RefSeq-defined human protein coding genes for analysis. Promoter was defined as the region from 2,500 base pair (bp) upstream to 500 bp downstream from the annotated transcript start site. Pseudogenes are known hot spots for artifacts due to their sequence similarity to their parent genes. In order to avoid potential variant calling bias, partially due to mapping difficulty, we removed the promoters and UTR analyses for pseudogenes.

Transcription factor binding sites (TFBS): TFBS information is based on data from ChIP-seq experiments performed by the ENCODE project (Consortium, 2012). ENCODE union TFBS regions processed by FunSeq (http://funseq2.gersteinlab.org/data/2.1.0) were analyzed in this study. The midpoint of each TFBS was determined by averaging the start and end position of the binding site.

DNA polymerase II: We used data from ChIP-seq experiments performed by the ENCODE project. The average value of uniform peak signals for 4 cell lines, K562, MCF10A, PBDE and Raji were used for analysis.

The epigenetic features of the genome were downloaded from Roadmap Epigenomics Project. For pan-cancer analysis, we used the data from integrative analysis of 111 reference human epigenomes (Roadmap Epigenomics et al., 2015). Chromatin accessibility (DNase-seq) and seven types of histone modifications (H3K4me1, H3K4me3, H3K27me3, H3K36me3, H3K9me3, H3K27ac and H3K9ac) data are included in downstream analysis. The epigenome identifier from release 9 of the compendium (Roadmap

Epigenomics et al., 2015) for each tumor types are shown below: breast (E028), esophagus (E079), kidney (E086), liver (E066), lung (E096), melanoma (E059 and E061), ovary (E097), pancreas (E098).

Patient-specific background mutation probability model

We used logistic regression model to estimate the background mutation probability for each genome site. The expected background mutation rates are modeled using genetic and epigenetic features that co-vary with the localized mutation rates. We removed CDS region and immunoglobin loci, and selected high-mappable regions from whole genome for the logistic regression model. Replication timing, genetic features, epigenetic features and patient ID information are included in the logistic regression model to calculate the expected patient-specific mutation rate for each genome site.

Poisson binomial model for mutation significance

We selected all single base substitutions with recurring frequency more than 3 and extended 5-bp left/right flank to get the 11bp regions as candidate clustered mutation regions. Noncoding mutation within 5kb of gene transcription start sites are further selected in downstream analysis. For each 11bp region, we calculated the mutation probability of each genome site using logistic regression model, then calculated the mutation probability for each 11bp region:

$$\Pr(\text{region is mutated}) = 1 - \prod_{i=1}^{11}(1 - p_i)$$

Here p_i is the mutation probability of genome site i within the 11bp region. Mutation recurrence in the given region of interest is then modeled using the Poisson binomial distribution, which accounts for variations in mutation rates across tumors. For a specific region of interest, the probability of having mutations in k or more individuals is calculated as following:

$$\Pr(K \geq k) = \sum_{m=k}^{n} \sum_{A \in F_m} \prod_{i \in A} p_i \prod_{j \in A^c} (1 - p_j)$$

Here, p_i and p_j are the region mutation probabilities for different patients, n is the total number of patients, k is the patient number with mutation in the given 11bp region. We used the R package “poibin” to calculate the *P* value for each 11bp region (Hong, 2013). The *P* values were then adjusted with Bonferroni method.

CDC20 promoter related database analysis

CDC20 mRNA expression analysis in pan-cancer: We used the Firebrowse database of Broad Institute to compare the mRNA expression difference between tumor and normal tissues in 37 cancer types. The mRNA expression levels are represented as normalized RSEM (log_2).

Survival analysis: TCGA SKCM patients were selected and divided into two groups, *CDC20* mRNA high and *CDC20* mRNA low, based on *CDC20* mRNA expression level. Kaplan-Meier overall survival curves were compared in these two groups. Log-rank test *P* value was reported. In ICGC MELA-AU project, we selected patients with mutation occurred in *CDC20* locus and nearby regions. Then we divided the patients into two groups, one group with mutation in *CDC20* promoter mutation hotspot region, another group with mutation occurred in *CDC20* locus but not in promoter mutation hotspot region. Kaplan-Meier overall survival curves were compared in these two groups.

ELK4 Chip-seq signal visualization: Two ELK4 Chip-Seq datasets including HeLa-S3 and HEK293 cell lines were queried by https://www.encodeproject.org/search/?searchTerm=ELK4&type=Dataset, bigWig files were downloaded and the ELK4 signals around CDC20 promoter were then plotted with R.

CDC20 promoter cloning and mutation

CDC20 promoter containing 859 bp upstream of the transcription start site was amplified from human genomic DNA with the primers 5'ATGCGGTACCGGCAGTCTAAGCTTATCTTCCAGATA3' and 5'ATGCCTCGAGGTGCTCAGGGGACAGAAAGGGACC3'. The amplified fragment was cloned into the mammalian expression vector pGL3 basic from Promega using the restriction enzymes KpnI and XhoI. The site directed mutations of *CDC20* promoter were created using the Fast Mutagenesis System from Transgen according to manufacturer`s protocol. The primers used for mutation are listed below:

525 F-5'CTGAGACTTTCCCCGAAAGGCCCGCCR3',
R-5'TCGGGGAAAGTCTCAGCTATCACGA3';

528 F- 5'AGACTTTCCCCGGAAAGCCCGCCCCC3',
R-5'TTTCCGGGGA AAGTCTCAGCTATCA3' ;

529 F-5'GACTTTCCCCGGAAGACCCGCCCCCT3',
R- 5'TCTTCCGGGG AAAGTCTCAGCTATC3'.

450-F: TCCTCTGGCGCTGGCTCCCAGC
R: GCTGGGAGCCAGCGCCAGAGGA

M514-F: TGATAGCTGAAACTTTCCCCGG
R: CCGGGGAAAGTTTCAGCTATCA
M583-F: GCGACGGTTAGATTTTGAAG
R: CTTCAAAATCTAACCGTCGC
All constructed vectors have been validated by sequencing.

Luciferase reporter assay

Five thousand cells (HEK293, M14) per well were co-transfected in 96-well format with wild type or mutant *CDC20* promoter driving pGL3 vector and Renilla plasmid as a normalization control. Forty eight hours after transfection the cells were washed with phosphate-buffered saline (PBS). The cells were then lysed in the luciferase lysis buffer provided with the Luciferase Assay Kit (Promega, Madison, USA). Luciferase activity was measured with the Dual-Luciferase Reporter Assay System (Promega). Values reported are firefly luciferase divided by Renilla luciferase. All cell lines were obtained from ATCC and were cultured in DMEM (Corning, Cellgro) plus 10% FBS (Gibco), 100 U/ml penicillin G and 100 μg/ml streptomycin (Corning, Cellgro). Each assay was done in duplicate and repeated for three times.

Quantitative PCR (Q-PCR) to quantify gene expression

Total RNA was extracted with TRIzol® Reagents (Invitrogen) according to the provided protocol. 1μg total RNA was reversed transcribed with iScript™ cDNA Synthesis Kit (Bio-Rad). Real time quantitative PCR was performed using diluted cDNA, SYBR® Green JumpStart™ Taq ReadyMix (Sigma) and appropriate primers in StepOnePlus Real Time PCR System (Applied Biosystems). Beta-actin was used as an endogenous control for normalization. Primer sequences for the following genes:

ACTB-rtF: CTCCATCCTGGCCTCGCTGT
ACTB-rtR: GCTGTCACCTTCACCGTTCC
CDC20-rtF: GACCACTCCTAGCAAACCTGG
CDC20-rtR: GGGCGTCTGGCTGTTTTCA
ETV3-rtF: GGTGGAGGGTATCAGTTTCCT
ETV3-rtR TGATGAATGGGTAGTTGGGCAT
ELK1-rtF TCCCTGCTTCCTACGCATACA
ELK1-rtR GCTGCCACTGGATGGAAACT
ELK3-rtF ATCTGCTGGACCTCGAACGA
ELK3-rtR TTCTGCCCGATCACCTTCTTG
ELK4-rtF ACTCAGCCGAGCCCTCAG
ELK4-rtR GGTGGCTTTTTGGAAGGTG

EFR-rtF GCAAGCCCCAGATGAATTACG
EFR-rtR CCCCTTGGTCTTGTGCAGAA
ETV6-rt-F AGGCCATCCGTGGATAATGTG
ETV6-rt-R CGGTGATTTGTCGTGATAGGTGA

Cell culture and DNA damage induction

M14, HEK293, 7721, A375 cells were purchased from American Type Culture Collection and cultured in DMEM supplemented with 10% FBS and 1% penicillin and streptomycin and maintained in an atmosphere of 5% CO2 at 37 °C. Transient transfections were done with various expression plasmids in different cell lines using Lipofectamine 2000 (Invitrogen). According to manufacturer's protocol and cells were harvested after 48 h. For DNA damage induction, cells were treated with 1 mg/ml of 5-fluoro uracil (5FU) (Sigma).

Chromatin immunoprecipitation

ChIP was performed as described previously (Liu et al., 2014; Nelson et al., 2006). Briefly, protein–DNA complexes were cross-linked for 10 min at room temperature with 1% formaldehyde added directly into the culture medium. The reaction was stopped by the addition of glycine (final concentration 0.125 mol/L) and incubated for 5 min with gentle rocking. The cells were washed with PBS and buffer (10 mM Tris at pH 8.0, 10 mM EDTA, 0.5 mM EGTA, 0.25% Triton-X-100), suspended in 200 mL of lysis buffer (1.1% Triton- X-100, 4 mM EDTA, 40 mM Tris at pH 8.1, 300mM NaCl), and submitted to sonication to produce small DNA fragments (200–1000 base pairs). Chromatin was precleared and immunoprecipitated with the anti-flag M2 beads (Sigma). Precipitated DNA and protein complexes were reverse-cross-linked, and DNA fragments were purified with a QIAquick PCR purification kit (Qiagen). The purified DNAs were quantified by real-time Q-PCR. Primers to quantify the abundance of human CDC20 promoter were as follows:

CDC20-chipF TCACATCTTTAAAGCCCCAA
CDC20-chipR GTTTTACAAACAGGGAAAAT

Lentiviral shRNA-mediated knockdown

Plasmids expressing shRNA were constructed by cloning double strand oligonucleotides into the pLKO.1 vector containing the puromycin resistance gene. Lentiviral shRNA-mediated knockdown was performed as described previously (Liu et al., 2014). The oligonucleotides used for shRNA are listed

below:

ELK1-F

CCGGCCCAAGAGTAACTCTCATTATCTCGAGATAATGAGAGTTACTCTTGGGTTTTTTGGTACC

ELK1-R AATTGGTACCAAAAAACCCAAGAGTAACTCTCATTATCTCGAGATAATGAGAGTTACTCTTGGG

ETV6-F

CCGGCCATAAGAACAGAACAAACATCTCGAGATGTTTGTTCTGTTCTTATGGTTTTTTTGGTACC

ETV6-R

AATTGGTACCAAAAAACCATAAGAACAGAACAAACATCTCGAGATGTTTGTTCTGTTCTTATGGT

ETV3-F

CCGGCCTCAGATACTATTACAACAACTCGAGTTGTTGTAATAGTATCTGAGGTTTTTTGGTACC

ETV3-R

AATTGGTACCAAAAAACCTCAGATACTATTACAACAACTCGAGTTGTTGTAATAGTATCTGAGG

ERF-F

CCGGGAGGTGACTGACATCAGTGATCTCGAGATCACTGATGTCAGTCACCTCTTTTTTGGTACC

ERF-R

AATTGGTACCAAAAAAGAGGTGACTGACATCAGTGATCTCGAGATCACTGATGTCAGTCACCTC

ELK4-F

CCGGGCCCAAGTATTTCTCCATCTTCTCGAGAAGATGGAGAAATACTTGGGCTTTTTTGGTACC

ELK4-R

AATTGGTACCAAAAAAGCCCAAGTATTTCTCCATCTTCTCGAGAAGATGGAGAAATACTTGGGC

ELK3-F

CCGGCTCCTCTTTAATGTTGCCAAACTCGAGTTTGGCAACATTAAAGAGGAGTTTTTTGGTACC

ELK3-R

AATTGGTACCAAAAAACTCCTCTTTAATGTTGCCAAACTCGAGTTTGGCAACATTAAAGAGGAG

Electrophoretic mobility shift assay (EMSA)

EMSA was performed using a chemiluminescent EMSA kit from Beyotime

Biotechnology following the manufacturer's instructions. Briefly, M14 cell nuclear extracts were prepared using NE-PER nuclear and cytoplasmic extraction reagents (ThermoFisher Scientific) according to the manufacturer's protocol. EMSA reactions included 1× binding buffer, 50 ng poly(dI-dC), 2.5% glycerol, 0.06% Nonidet P-40, 5 mM MgCl2, 19 μ g BSA, 2 μ l nuclear extract, and 20 fM biotin-labelled probes. Specificity of mobility shifts was analyzed by including un-labelled *CDC20* competitor oligonucleotides at the concentration of 8 pM. Reactions were incubated for 20 min at room temperature, size-separated on a 6% DNA retardation gel, and transferred to nylon membrane. Free or protein-bound biotin-labelled probes were detected using streptavidin–horseradish peroxidase conjugates and chemiluminescent substrate according to the manufacturer's protocol. Probe sequences for promoter regions are listed below:

WT F-5' ACTTTCCCCGGAAGGCCCGCCCCCT3'
R-5'AGGGGGCGGGCCTTCCGGGGAAAGT3'
525 F-5' ACTTTCCCCGAAAGGCCCGCCCCCT3'
R-5' AGGGGGCGGGCCTTTCGGGGAAAGT3'
528 F-5' ACTTTCCCCGGAAAGCCCGCCCCCT3'
R-5'AGGGGGCGGGCTTTCCGGGGAAAGT3'
529 F-5' ACTTTCCCCGGAAGACCCGCCCCCT3'
R-5'AGGGGGCGGGTCTTCCGGGGAAAGT3'

Supplemental References

Consortium, E.P. (2012). An integrated encyclopedia of DNA elements in the human genome. Nature *489*, 57-74.

Genomes Project, C., Auton, A., Brooks, L.D., Durbin, R.M., Garrison, E.P., Kang, H.M., Korbel, J.O., Marchini, J.L., McCarthy, S., McVean, G.A.*, et al.* (2015). A global reference for human genetic variation. Nature *526*, 68-74.

Hong, Y. (2013). On computing the distribution function for the Poisson binomial distribution. In Computational Statistics and Data Analysis, pp. 41-51.

Liu, X.S., Haines, J.E., Mehanna, E.K., Genet, M.D., Ben-Sahra, I., Asara, J.M., Manning, B.D., and Yuan, Z.M. (2014). ZBTB7A acts as a tumor suppressor through the transcriptional repression of glycolysis. Genes Dev *28*, 1917-1928.

Nelson, J.D., Denisenko, O., and Bomsztyk, K. (2006). Protocol for the fast chromatin immunoprecipitation (ChIP) method. Nat Protoc *1*, 179-185.

Roadmap Epigenomics, C., Kundaje, A., Meuleman, W., Ernst, J., Bilenky, M., Yen, A., Heravi-Moussavi, A., Kheradpour, P., Zhang, Z., Wang, J.*, et al.* (2015). Integrative analysis of 111 reference human epigenomes. Nature *518*, 317-330.

Siepel, A., Bejerano, G., Pedersen, J.S., Hinrichs, A.S., Hou, M., Rosenbloom, K., Clawson, H., Spieth, J., Hillier, L.W., Richards, S.*, et al.* (2005). Evolutionarily conserved elements in vertebrate, insect, worm, and yeast genomes. Genome Res *15*, 1034-1050.